A Predistorter for an AM-VSB Lightwave CATV System

by

Andrew Keir

B.A.Sc., Simon Fraser University, 1992

THESIS SUBMITTED IN PARTIAL FULFILMENT

OF THE REQUIREMENTS FOR THE DEGREE OF

MASTER OF APPLIED SCIENCE

in the School of Engineering Science

SIMON FRASER UNIVERSITY

August 10, 1993

ISBN 0-315-91203-0

APPROVAL

NAME: Andrew Keir

DEGREE: Master of Applied Science (Engineering Science)

TITLE OF THESIS: A Predistorter for an AM-VSB Lightwave CATV System

EXAMINING COMMITTEE:

Chairman:

Dr. John Jones, P.Eng.
Associate Professor
School of Engineering Science, SFU

Senior Supervisor:

Dr. Shawn Stapleton, P.Eng.
Associate Professor
School of Engineering Science, SFU

Committee Member:

Dr. Andrew Rawicz
Associate Professor
School of Engineering Science, SFU

External Examiner:

Dr. C.J. Chung
Staff Scientist
Photon Systems Corp, Burnaby, B.C.

DATE APPROVED: 9 AUGUST 1993

PARTIAL COPYRIGHT LICENSE

I hereby grant to Simon Fraser University the right to lend my thesis, project or extended essay (the title of which is shown below) to users of the Simon Fraser University Library, and to make partial or single copies only for such users or in response to a request from the library of any other university, or other educational institution, on its own behalf or for one of its users. I further agree that permission for multiple copying of this work for scholarly purposes may be granted by me or the Dean of Graduate Studies. It is understood that copying or publication of this work for financial gain shall not be allowed without my written permission.

Title of Thesis/Project/Extended Essay

"A Predistorter for an AM-VSB Lightwave CATV System"

Author:

(signature)

Andrew KEIR
(name)

August 9, 1993
(date)

ABSTRACT

A wideband predistorter for an AM-VSB Lightwave CATV system was analyzed and implemented. The laser and predistorter were modeled as third order polynomials with real coefficients which produce only AM/AM distortion. Based on this model, analytical expressions showing the improvement in the composite second order and composite triple beat using predistortion were derived. Also, a measurement technique for obtaining the coefficients of the laser and the predistorter is described. A predistorter was then designed and constructed using discrete schottky diodes. The predistorter was able to reduce the second order non-linearity of a direct feedback (DFB) laser by up to 12 dB in a 40 channel system, and the results also show how the predistorter could be controlled adaptively.

ACKNOWLEDGEMENTS

I would like to thank Dr. Shawn Stapleton for his help and guidance throughout this thesis. Our numerous discussions were much appreciated. Thanks also to Sirooj Rambaran for his help and expertise in tracking down 'RF problems'. His knowledge of practical testing techniques was invaluable.

Also, thank-you to John Maycock and the gang down at Photon Systems Corp. for providing us with the laser transmitter and optical receiver used in this work. The use of the matrix generator was also appreciated.

Tracy deserves special thanks for her support and understanding throughout my studies. Research does strange things to a person's mind.

Finally, I would like to thank the members of the RF/Microwave group; Trent, Le, and Wen-lei, for providing an enjoyable working environment.

Table of Contents

Table of Figures

Table of Tables

LIST OF ABBREVIATIONS

α_1	first order predistorter coefficient
α_2	second order predistorter coefficient
α_3	third order predistorter coefficient
β_1	first order laser coefficient
β_2	second order laser coefficient
β_3	third order laser coefficient
ζ_1	first order composite coefficient
ζ_2	second order composite coefficient
ζ_3	third order composite coefficient
A/D	analog to digital
AM	amplitude modulation
AM-VSB	amplitude modulation with vestigial sidebands
B_1	lower bandwidth for white noise source
B_2	upper bandwidth for white noise source
CATV	cable television
CNR	carrier to noise ratio
CSO	composite second order
CTB	composite triple beat
D/A	digital to analog
dBc	power in dB relative to the carrier
dBm	power in dB relative to 1 mW
DFB Laser	direct feedback laser
FM	frequency modulation

m	modulation index per channel
N	number of channels
NLD	non-linear distortion
N_o	white noise power level
RIN	relative intensity noise
TDM	time division multiplexing
$V_a(t)$	composite output signal
$V_d(t)$	predistorter output signal
$V_l(t)$	laser output signal
$V_m(t)$	input signal

1 INTRODUCTION

In recent years, the cable television industry has undergone major changes. With the advent of suitable lasers and fibre optic equipment, many existing coaxial cable distribution networks are being replaced with fibre optic networks. These new optical distribution systems result in considerably better television pictures transmitted to the customer and also provide the capability to bring many other services to the customer that were not possible using cable.

The most common type of optical CATV distribution system uses AM modulation to transmit the CATV signals. Therefore, the laser must be highly linear so that intermodulation distortion caused by non-linearities in the laser is kept to a minimum.

In CATV systems, intermodulation distortion is measured in terms of the composite second order (CSO) and composite triple beat (CTB). The CSO and CTB are the result of the power addition of all the second and third order beats at the particular frequency of interest. In terms of the actual CATV signal, the CSO interferes with the luminance information and the CTB interferes with the carrier. High levels of CSO and/or CTB result in visible distortion to the viewer.

The laser is the major limiting component in terms of the resulting CSO and CTB levels. In order to improve the CSO and CTB levels, the laser must be linearized. A number of linearization techniques have been investigated for use with optical systems. These methods include feedforward [1,2], quasi-feedforward [3], and predistortion [4,5,6]. Of these linearization techniques, predistortion appears to be the most cost effective technique. This is because feedforward techniques require two lasers, whereas predistortion only requires one. With predistortion, the input signal is passed through a predistorter that has the inverse non-linear characteristics of the laser diode. Therefore, when the predistorted signal is passed into the laser, the non-linearities will cancel each other and the resultant non-linear distortion (CSO and CTB) will be reduced.

Although literature on predistortion is already available, this work was carried out since there was very little information on how to build and test a wideband predistorter, and on the related theory. Also, little analysis had been completed which showed analytically the improvements one should obtain if predistortion is used in a CATV application. Furthermore, the analysis presented here analytically shows how predistortion

could be controlled adaptively using simple measurements of the distortion power. Previous adaptive predistorters required the use of additional test frequencies to adaptively control the linearization [6].

To this end, this thesis has been broken up into six sections. In Section 2, background information on optical CATV systems, how they work, and the major components are described. Also, linearization techniques for wideband systems are discussed.

Section 3 presents the analysis of the predistorter and laser system. The laser and predistorter characteristics are modeled as third order polynomials with real coefficients. From this model, expressions relating to the CSO and CTB are derived, as is an expression showing the improvement from predistortion. These expressions are then compared to the clipping distortion model to determine the practical limits of the predistorter.

The next section, Section 4, provides a mathematical description of how the predistorter was constructed using discrete schottky diodes. Also, expressions showing the amount of cancellation the predistorter can achieve when amplitude and phase imbalances are present are shown.

Section 5 discusses how the predistorter was constructed and explains a test procedure used to determine the phase of the signals. The phase measurements were important because they were used to determine the sign of the polynomial coefficients. Preliminary tests were then performed on the predistorter using a schottky diode to model the laser. These tests verified that the predistorter was operating according to theory. Then, the predistorter was modified so that it could predistort a direct feedback (DFB) laser.

Section 6 presents the results of the predistorted laser. The predistorter was able to reduce the second harmonic of the laser between 90 -250 MHz by 3 to 20 dB. This resulted in a reduction in the CSO of up to 12 dB in a 40 channel system. Also, the modifications necessary to make the predistorter operate adaptively are shown.

Finally, Section 7 presents the conclusions and recommendations for further work. The results of this thesis indicate that wideband predistortion is possible. In a CATV system, both the second and third order distortion can be reduced, provided that the laser is operated in a region where clipping distortion does not dominate and the distortion signal

levels are large enough to make predistortion practical. Also, the predistortion technique used lends itself well to adaptive control based on power measurements of the distortion produced. Finally, this work will be very useful for any designer investigating the possibility of using predistortion for any wideband application.

2 BACKGROUND

This section contains a brief review of the important parts of a CATV lightwave system and the associated terminology. Also, aspects of linearization schemes will be discussed.

2.1 CATV Lightwave Systems

A CATV lightwave system consists of a laser diode, which transmits the CATV signals, optical fibre, which provides the signal channel, and a PIN photodiode, which converts the optical signals back into electrical signals. Figure 2.1.1 shows a block diagram of the complete system.

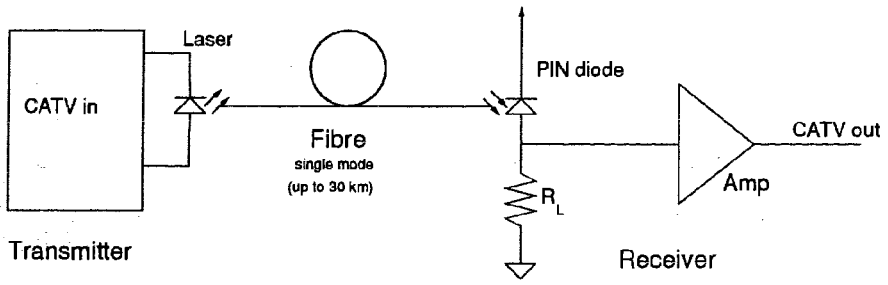

Figure 2.1.1: Block Diagram of CATV Lightwave System

There are two methods of transmitting the CATV signals over optical fibre: digital transmission, and analog transmission. Digital transmission currently uses TDM (time division multiplexing) techniques which result in excellent performance. However, digital transmission has the drawbacks of being complex and expensive, and since the consumer's TV requires an AM-VSB analog input, A/D and D/A conversion is required at the input and output of the system [7].

Analog transmission of CATV signals over optical fibre has been achieved using both AM and FM formats. FM transmission provides good performance, but like the digital system, the FM system requires a converter to produce the AM-VSB signal after the optical receiver [7]. AM transmission uses the same AM-VSB format currently employed in existing cable systems. Thus, the signals coming into or out of an AM fibre system can feed directly into a coaxial system. This is a tremendous benefit, as it

means that AM fibre systems can be introduced slowly, without having to replace the entire system all at once. Also, the analog fibre system is very simple which makes it inexpensive to produce, and the performance, although not as good as a digital system, is considerably better than that of the existing cable system [7].

The two most important components of the optical system are the laser diode and the photodiode. A brief description of each device is provided and then a summary of the optical link design trade-offs is given.

2.1.1 Laser Diodes

Laser diodes provide an optical output power that is proportional to the input bias current. Over a small range of bias currents, the optical output power vs input current is almost linear. Thus, if the bias current is modulated around this linear bias point, then the modulation in the optical output power can be used to transmit information. The modulation index, m, of the laser, refers to the amount of change in the optical intensity about the average optical intensity at the bias point. In optical CATV systems, the modulation index per channel is usually provided in the system specifications rather than the total amount of modulation in the laser for the composite channels.

The bias point must be chosen such that it provides the best possible carrier to noise ratio (CNR) and the lowest amount of intermodulation distortion. The CNR is limited by the combined effect of the residual intensity noise (RIN) of the laser and the intermodulation distortion. The RIN is a result of fluctuations in the output optical intensity of the laser and is specific to any given laser [8]. The CNR for a given optical length and input power is also a function of the RIN and the intermodulation noise.

The intermodulation distortion is caused by slight non-linearities in the laser light-current curve at the bias point, and in a multi-channel system, results in the formation of CSO and CTB. By linearizing the laser, this distortion can be reduced.

The most common type of laser used in CATV applications is the distributed feedback (DFB) laser. These lasers oscillate at a single wavelength, typically 1300

nm for CATV applications. The DFB laser is quite temperature sensitive; for a fixed bias current, the optical power will increase with a decrease in temperature [9]. Therefore, the laser must be kept at a fixed temperature.

Other lasers, such as Fabry-Perot, and V-Groove lasers have also been used in CATV systems [1,6]. These lasers are less common, but share the same characteristics as DFB lasers in that they have a given RIN value and a slightly non-linear light-current curve that results in intermodulation distortion [8].

Therefore, any of the lasers used in CATV systems can be linearized using some linearization technique. Predistortion will apply to all types of lasers.

2.1.2 Photodiodes

Photodiodes convert an optical input signal into an electrical current. The electrical current is directly proportional to the optical input power. Most CATV applications use PIN diodes which have no internal gain as opposed to APD (avalanche) photodiodes which have an internal gain. This is because the extra gain from APD's is not needed and it increases the system noise [9]. Also, APD's produce higher intermodulation distortion than PIN diodes.

PIN diodes are made of InGaAs (indium-gallium-arsenide) for 1300 nm systems [9]. The important specifications of PIN diodes are the responsivity, the dark current, and the internal capacitance. The responsivity is a measure of the conversion from optical input power to output current in A/W. For CATV applications, a responsivity of at least 0.82 A/W is required.

The dark current is the reverse current that flows in the photodiode when no input is present. This current must be small to allow for the detection of small input signals. The dark current increases with temperature which means that the sensitivity of the photodiode decreases with temperature.

Finally, the internal capacitance of the photodiode limits the bandwidth of the system. The internal capacitance is typically 1 pF or smaller, which means that the normalized 3 dB bandwidth is 3 GHz with a 50 ohm load.

PIN photodiodes for CATV applications, like the laser diodes, must have a linear light-current characteristic or they will cause intermodulation distortion. The distortion caused by a PIN diode is considerably smaller than the distortion caused by a laser and is generally not a limiting factor.

2.1.3 Link Design Trade-offs

In the complete optical link, different parts of the system limit the overall performance depending on the length of the fibre or corresponding amount of optical loss. Single mode optical fibre typically has a loss of approximately 0.4 dB/km at a wavelength of 1300 nm.

For small amounts of optical loss, the CNR may be limited by either the receiver (PIN diode) or the laser. In the laser, the upper CNR limit is fixed by the RIN, and then additional noise is created at the receiver from thermal noise, PIN diode shot noise, and the receiver amplifier internal noise which sets the system noise floor [7,8]. In general, if the signal levels incident to the photodiode are large, then the CNR will be high. Unfortunately, the large signal levels incident on the receiver may cause the receiver to produce intermodulation distortion in excess of the lasers intermodulation distortion. This excess distortion is caused by non-linearities in the receiver amplifiers which becomes noticeable only at large input powers. If the input power is attenuated at the receiver before the amplifiers, the distortion will be reduced but the CNR will degrade.

The amount of intermodulation distortion coming from the laser depends on the input power to the laser, which is directly related to the modulation index at the input. For large modulation indices, the distortion will be large. Thus, if the optical loss is high, then the input power incident at the receiver will be low enough that the receiver amplifiers do not increase the distortion already coming from the laser. This means that the distortion measured at the receiver will be from the laser only. However, the CNR will be lower since the receivers noise floor is fixed and the input power is smaller. Therefore, when specifying an optical AM-VSB CATV system, the CNR vs intermodulation distortion trade-off must be carefully examined.

2.2 Linearization Techniques

There are a variety of linearization techniques that can be used to linearize a given non-linear device. For wideband systems, two methods are frequently used; feedforward linearization and predistortion linearization.

2.2.1 Feedforward Linearization

Feedforward linearization involves taking a delayed version of the input signal and comparing it to the corresponding non-linear device output signal to generate an error signal. The error signal is then amplified and subtracted from the non-linear device output to eliminate the non-linearities.

For CATV systems, feedforward linearization has been investigated [1,2,3]. Although the feedforward technique works well, it is very expensive. This is because two lasers, an optical splitter, and an optical combiner are required. Figure 2.2.1 shows a block diagram of a feedforward linearizer for a laser diode.

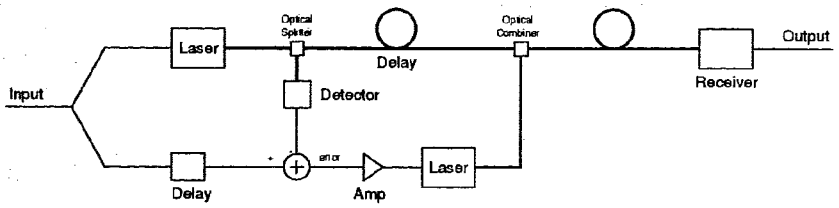

Figure 2.2.1: Feedforward Linearization

The optical laser output contains non-linearities, so a portion of the optical signal is redirected from the main path into an optical detector. The detector converts the optical output into an electrical signal which is compared to the corresponding input signal to create the error signal. The delay in the electrical path is adjusted to account for the signal delay through the laser, fibre, and detector. The error signal is then amplified, transmitted by the second laser, and combined optically with an optical combiner to cancel the non-linearities from the first laser. An additional optical delay is required on the original laser's optical path so that the error signal adds with the correct phase relationship.

This linearization method is sensitive to the delay devices since cancellation will not occur if the error signal does not have the correct phase relationship with the original signal.

2.2.2 Predistortion Linearization

Predistortion linearization involves constructing a predistorter which has the inverse non-linear characteristics of the non-linear device. Thus, when the predistorter's output signal is passed through the non-linear device, the distortion components cancel and the output remains linear. Figure 2.2.2 shows a block diagram of a predistortion linearizer.

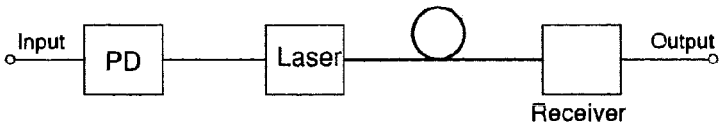

Figure 2.2.2: Predistortion Linearization

Unlike feedforward, only the laser producing the non-linear distortion is required in a predistortion system; the error signal is an electrical signal applied to the input of the laser. Thus, predistortion is a more cost effective technique.

Predistortion has been applied successfully to a number of Lightwave CATV systems [4,5,6]. In most cases, either the second order distortion of a DFB laser or the third order distortion caused by an external modulator was reduced. Most of the predistorters were static predistorters and therefore did not adapt to changes in the performance of the system.

Since the laser and other active components will drift over time, a more robust predistorter is one that adapts the predistorter output to account for component changes over time. One predistortion system in the literature was adaptive [6], and it used additional test tones to produce an error signal to control the adaptive loop. However, this method was rather complex and suffered from potential instability problems due to the use of analog integrators.

This work describes a simple method for building a predistorter and a simple method to control the predistorter adaptively using measurements of the distortion power. No additional test signals are required, and the control loop, although possessing a slow convergence time, will be adequate for long-term stability.

3 ANALYSIS

This section provides an analysis of the expected laser behaviour using a third order polynomial model. A third order model was used because it reduces the complexity of the analytical expressions and because it has been found to describe laser non-linearities with good results [10,11]. Previous papers have either explicitly or implicitly used this model for building a predistorter, but little analysis has been given.

The analysis provides a complete description of the polynomial model and it results in an expression that specifies the level of the CSO and CTB caused by the laser non-linearities in a multi-channel system. The amount of improvement attainable using predistortion and a simple method for controlling the predistorter adaptively are shown. Furthermore, the limits of the polynomial model in terms of the potential improvement by a predistorter are shown by taking signal clipping into account.

3.1 Polynomial Model

The laser light-current curve (L-I curve) is approximated by a third order power series with real coefficients β_1, β_2 and β_3. The non-linearities are assumed to be memoryless with only AM/AM distortion. Therefore, no frequency dependent distortion will take place. This assumption is based on the input frequencies being low compared to the lasing frequency of the laser. If frequency dependent distortion occurs, predistortion becomes considerably more difficult since specific components would be required to shift the phase appropriately for each frequency.

The predistorter is also approximated by a third order power series with real coefficients α_1, α_2, and α_3. The composite system is a cascade of the predistorter and the laser as shown in Figure 3.1.1. Equations (3.1.1) - (3.1.3) show the signal dependencies given that $V_m(t)$ is the input signal, $V_d(t)$ is the predistorter output, and $V_l(t)$ is the laser output. $V_a(t)$ is the composite output.

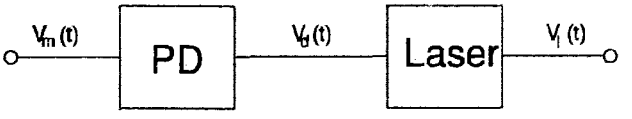

Figure 3.1.1: Block Diagram of Predistorter

$$V_d(t) = V_m(t) \cdot \{\alpha_1 + \alpha_2 \cdot V_m(t) + \alpha_3 \cdot |V_m(t)|^2\}. \quad (3.1.1)$$

$$V_l(t) = V_d(t) \cdot \{\beta_1 + \beta_2 \cdot V_d(t) + \beta_3 \cdot |V_d(t)|^2\}. \quad (3.1.2)$$

$$V_a(t) = V_m(t) \cdot \{\zeta_1 + \zeta_2 \cdot V_m(t) + \zeta_3 \cdot |V_m(t)|^2\}. \quad (3.1.3)$$

The values of the ζ'*s* in (3.1.3) in terms of the α'*s* and β'*s* are

$$\begin{aligned} \zeta_1 &= \alpha_1\beta_1, \quad (3.1.4) \\ \zeta_2 &= \alpha_1^2\beta_2 + \alpha_2\beta_1, \\ \zeta_3 &= \alpha_1^3\beta_3 + 2\alpha_1\alpha_2\beta_2 + \alpha_3\beta_1, \end{aligned}$$

where only terms involving the first, second, and third order values have been kept. The higher order terms resulting from the cascade of the predistorter and the laser are assumed to be much smaller than the first three terms.

From (3.1.4), the optimum predistorter coefficients that will result in the elimination of the second and third order distortion are

$$\hat{\alpha}_2 = -\frac{\alpha_1^2\beta_2}{\beta_1}, \quad (3.1.5)$$

$$\hat{\alpha}_3 = -\frac{(\alpha_1^3\beta_3 + 2\alpha_1\hat{\alpha}_2\beta_2)}{\beta_1}. \quad (3.1.6)$$

The optimum predistorter requires independent generation of both the second and third order coefficients. This relates directly to a device that produces independent second and third order distortion. Since the predistorter is to be realized using discrete diodes, the second order distortion generator will also produce some third order distortion and vice versa due to the non-ideal characteristics of the diodes. Care must be taken to avoid or compensate for this effect.

3.1.1 Autocorrelation Function

Typically, CATV systems transmit between N = 40 to 80 channels. The input CATV signal can therefore be approximated as a Gaussian distribution of N independent random variables when N > 10 by the central limit theorem [12]. If the CATV signal is also assumed to be a zero-mean wide sense stationary process, the autocorrelation function of the composite output $V_a(t)$ is defined as

$$R_a(\tau) = \frac{1}{2}\cdot E\{V_a(t)\cdot V_a^*(t-\tau)\}, \tag{3.1.7}$$

where $V_a^*(t)$ represents the complex conjugate of $V_a(t)$. Although the input signal appears on top of a DC bias in the laser, the input signal and the final output signal have no DC offsets involved, hence the signals are zero mean.

The output complex envelope from (3.1.3) is then

$$V_a(t) = V_m(t)\cdot\{\zeta_1+\zeta_2\cdot V_m(t)+\zeta_3\cdot|V_m(t)|^2\}, \tag{3.1.8}$$

$$V_a^*(t-\tau) = V_m^*(t-\tau)\cdot\{\zeta_1^*+\zeta_2^*\cdot V_m^*(t-\tau)+\zeta_3^*\cdot|V_m(t-\tau)|^2\}. \tag{3.1.9}$$

For convenience, denote $V_m(t)$ by V_1 and $V_m(t-\tau)$ by V_2. Expanding the argument of the expected value function in (3.1.7) in terms of V_1 and V_2 using (3.1.8) and (3.1.9), the autocorrelation function becomes

$$\begin{aligned} 2R_a(\tau) = {} & \zeta_1\zeta_1^*E\{V_1V_2^*\}+\zeta_1\zeta_2^*E\{V_1V_2^{*2}\}+\zeta_1\zeta_3^*E\{V_1V_2V_2^{*2}\} \\ & +\zeta_2\zeta_1^*E\{V_1^2V_2^*\}+\zeta_2\zeta_2^*E\{V_1^2V_2^{*2}\}+\zeta_2\zeta_3^*E\{V_1^2V_2V_2^{*2}\} \\ & +\zeta_3\zeta_1^*E\{V_1^2V_1^*V_2^*\}+\zeta_3\zeta_2^*E\{V_1^2V_1^*V_2^{*2}\}+\zeta_3\zeta_3^*E\{V_1^2V_1^*V_2V_2^{*2}\}, \end{aligned} \tag{3.1.10}$$

where $|V_m(t)|^2 = V_1V_1^*$ and $|V_m(t-\tau)|^2 = V_2V_2^*$.

The expected values appearing in (3.1.10) can be determined using the following formula for the mixed moments of L zero-mean jointly Gaussian random variables $x_1, x_2, \ldots, x_L$ [13]

$$E\{x_1,x_2,\ldots,x_L\} = \begin{cases} 0 & \text{if L is odd} \\ \sum_{\text{all distinct pairs of subscripts}} [\lambda_{ij}\lambda_{lm}\ldots\lambda_{nL}] & \text{if L is even} \end{cases} \tag{3.1.11}$$

where $\lambda_{lk} = E\{x_lx_k\}$.

For example, $E\{x_1x_2x_3x_4\} = \lambda_{12}\lambda_{34}+\lambda_{13}\lambda_{24}+\lambda_{14}\lambda_{23}$.

If some of the variables appear in the moment expression with a power of 2 or higher, each repeated subscript is treated as if it were distinct when applying the formula.

From (3.1.10), the expected values with odd powers will be zero using (3.1.11). To calculate the remaining five expected values, make the substitution

$$V_1 = x_1 + jy_1, \tag{3.1.12}$$

$$V_2^* = x_2 - jy_2. \tag{3.1.13}$$

Since $V_m(t)$ is zero mean, both x(t) and y(t) are zero mean as well. The autocorrelation and cross-correlation functions of the processes are given by

$$R_{xx}(\tau) = E\{x(t)x(t-\tau)\}, \tag{3.1.14}$$

$$R_{xy}(\tau) = E\{x(t)y(t-\tau)\}. \tag{3.1.15}$$

Using the properties of autocorrelation and cross-correlation [14], it can be shown that

$$\begin{aligned}
&E\{x_1x_1\} = E\{x_2x_2\} = E\{y_1y_1\} = E\{y_2y_2\} = R_{xx}(0), \\
&E\{x_1y_1\} = E\{y_1x_1\} = E\{x_2y_2\} = E\{y_2x_2\} = 0, \\
&E\{x_1x_2\} = E\{x_2x_1\} = E\{y_1y_2\} = E\{y_2y_1\} = R_{xx}(\tau), \\
&E\{x_1y_2\} = E\{y_2x_1\} = R_{xy}(\tau), \\
&E\{x_2y_1\} = E\{y_1x_2\} = R_{yx}(\tau).
\end{aligned} \tag{3.1.16}$$

It can also be shown that [14]

$$R_m(\tau) = R_{xx}(\tau) - jR_{xy}(\tau). \tag{3.1.17}$$

For example, expanding the term $E\{V_1V_2V_2^{*2}\}$ results in

$$\begin{aligned}
E\{V_1V_2V_2^{*2}\} = E\{&x_1x_2^3 + x_2^2y_1y_2 + x_1x_2y_2^2 + y_1y_2^3 \\
&+ j[-x_1y_2^3 + x_2y_1y_2^2 - x_1x_2^2y_2 + x_2^3y_1]\}.
\end{aligned} \tag{3.1.18}$$

Each expected value is then determined using (3.1.11). For example,

$$E\{x_1x_2^3\} = E\{x_1x_2\}\cdot E\{x_2x_2\}+E\{x_1x_2\}\cdot E\{x_2x_2\} \quad (3.1.19)$$
$$+E\{x_1x_2\}\cdot E\{x_2x_2\}$$
$$= 3R_{xx}(0)\,R_{xx}(\tau).$$

When each of the terms in (3.1.18) is expanded and evaluated as in (3.1.19), the sum is $8R_{xx}(0)R_m(\tau)$. The same substitutions and expansions are carried out for the remaining terms in (3.1.10). Using (3.1.17) to convert from R_{xx} and R_{xy} to R_m results in

$$R_a(\tau) = [|\zeta_1|^2+8|\zeta_1\zeta_3|R_m(0)+16|\zeta_3|^2R_m^2(0)]R_m(\tau) \quad (3.1.20)$$
$$+4|\zeta_2|^2R_m^2(\tau)+8|\zeta_3|^2R_m^3(\tau).$$

The power spectral density function $S_m(f)$ of the complex envelope $V_m(t)$ is obtained by taking the Fourier transform of its autocorrelation function $R_m(\tau)$,

$$S_m(f) = \int_{-\infty}^{+\infty} R_m(\tau)e^{-j2\pi f\tau}d\tau. \quad (3.1.21)$$

Using the convolution theorem, the power spectral density of the CATV output is

$$S_a(f) = |\zeta_1|^2S_m(f)+4|\zeta_2|^2S_m(f)\otimes S_m(f) \quad (3.1.22)$$
$$+8|\zeta_3|^2S_m(f)\otimes S_m(f)\otimes S_m(f),$$

where $\otimes$ denotes convolution. In (3.1.22), the $|\zeta_1\zeta_3|$ and the $|\zeta_3|^2$ terms have been dropped from the $R_m(\tau)$ term since the $|\zeta_1|^2$ term will dominate provided that $\zeta_2 \ll \zeta_1$, and $\zeta_3 \ll \zeta_1$.

3.1.2 Power Spectrum

To obtain the power spectral density $S_a(f)$, the convolutions of the input $S_m(f)$ must be performed. Let $S_m(f)$ be a constant $N_o/2$ over the bandwidth B_1 to B_2, where for a CATV system B_1 = 50 MHz and B_2 = 450 MHz (60 channels). The PSD is also assumed to be two-sided and the broadcast FM band is ignored. The FM band

encompasses the frequencies between 88 MHz and 108 MHz, but the closest CATV signal carriers occur at 83.25 MHz and 121.25 MHz. Figures 3.1.2a to 3.1.2c show the input spectrum $S_m(f)$ and the convoluted spectra $S_m(f) \otimes S_m(f)$ and $S_m(f) \otimes S_m(f) \otimes S_m(f)$ where $N_o = 2$.

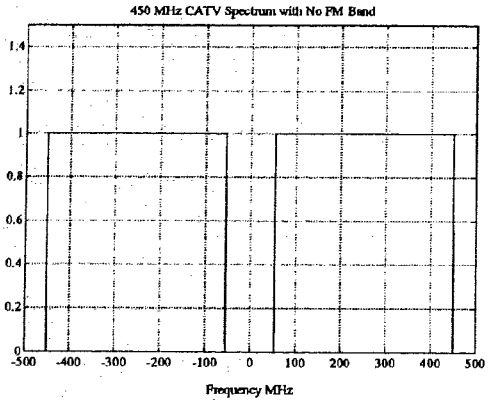

Figure 3.1.2a: $S_m(f)$

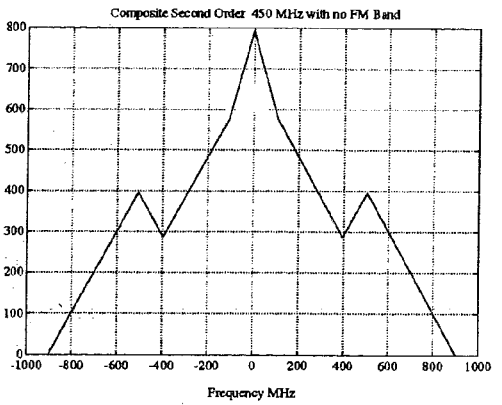

Figure 3.1.2b: $S_m(f) \otimes S_m(f)$

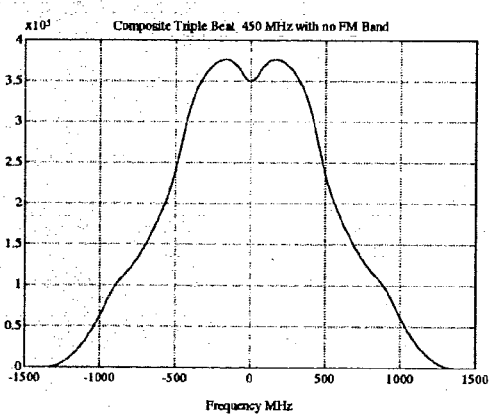

Figure 3.1.2c: $S_m(f) \otimes S_m(f) \otimes S_m(f)$

From Figure 3.1.2, the 2nd order distortion is highest at the lower end of the band and has a peak at the upper end of the band. The 3rd order distortion is highest near the centre of the band. This is in agreement with the standard CATV measurements using beat counts.

Analytical expressions can be obtained for the convolution spectra shown in Figure 3.1.2. The second order convolution is broken down into four sections from $-2B_2$ to 0. They are

$$\begin{aligned} S_2(w) &= \frac{N_o^2}{4}\cdot(w+2B_2) && -2B_2 \le w \le -(B_1+B_2) \\ S_2(w) &= \frac{N_o^2}{4}\cdot(-w-2B_1) && -(B_1+B_2) \le w \le -B_2+B_1 \\ S_2(w) &= \frac{N_o^2}{2}\cdot(B_2-B_1+w)+\frac{N_o^2}{4}\cdot(-w-2B_1) && -B_2+B_1 \le w \le -2B_1 \\ S_2(w) &= \frac{N_o^2}{2}\cdot(B_2-B_1+w) && -2B_1 \le w \le 0. \end{aligned} \tag{3.1.23}$$

Similar expressions can be derived for the third order convolution. There are 8 separate terms from $-3B_2$ to 0 and the expressions are quite complex. The maximum value of the convolution occurs at $-3B_1$ and is

$$S_3(w)_{\max} = \frac{3N_o^3}{8}\cdot(B_2^2-4B_1B_2+7B_1^2). \tag{3.1.24}$$

The maximum contribution of the 2nd order distortion in the CATV band occurs on channel 4 at the low end of the band. The 2nd order distortion is also large at the upper end of the band. A good approximation between the distortion at the lower and upper ends of the band uses the second order convolution value just above the high end of the band ($w = -(B_2+B_1)$). Using the analytical value for the convolution at this point from (3.1.23) results in the second term of (3.1.22) becoming

$$P_2 = 4\cdot|\zeta_2|^2\cdot\frac{N_o^2}{4}\cdot(B_2-B_1). \tag{3.1.25}$$

The maximum contribution of the 3rd order distortion occurs in the centre of the band and using the analytical value for the convolution results in the third term of (3.1.22) becoming

$$P_3 = 8 \cdot |\zeta_3|^2 \cdot \frac{3N_o^3}{8} \cdot (B_2^2 - 4B_1B_2 + 7B_1^2). \tag{3.1.26}$$

The power of the input spectrum or the first term of (3.1.22) becomes

$$P_1 = |\zeta_1|^2 \cdot \frac{N_o}{2}. \tag{3.1.27}$$

If the worst distortion in each of the terms P_1, P_2, and P_3 is added together, the result is a slightly overestimated worst case approximation of equation (3.1.22). Let S_{worst} be

$$S_{worst} = P_1 + P_2 + P_3, \tag{3.1.28}$$

or

$$S_{worst} = |\zeta_1|^2 \frac{N_o}{2} + |\zeta_2|^2 N_o^2 (B_2 - B_1) + |\zeta_3|^2 3N_o^3 (B_2^2 - 4B_1B_2 + 7B_1^2). \tag{3.1.29}$$

Thus, the worst case expressions for the CSO and CTB can be obtained;

$$CSO = \frac{P_2}{P_1} = 2 \cdot \frac{|\zeta_2|^2}{|\zeta_1|^2} \cdot N_o \cdot (B_2 - B_1), \tag{3.1.30}$$

$$CTB = \frac{P_3}{P_1} = 6 \cdot \frac{|\zeta_3|^2}{|\zeta_1|^2} \cdot N_o^2 \cdot (B_2^2 - 4B_1B_2 + 7B_1^2). \tag{3.1.31}$$

The system non-linear distortion power (NLD) is obtained by combining the 2nd and 3rd order distortion powers,

$$NLD = CSO + CTB. \tag{3.1.32}$$

An adaptive predistorter relies on the distortion power being a well behaved monotonically decreasing function with respect to the predistorter's coefficients. Expanding equation (3.1.32) to include the laser and predistorter coefficients results in

$$NLD = \frac{2N_o \cdot (B_2 - B_1) \cdot (\alpha_1^2\beta_2 + \alpha_2\beta_1)^2}{(\alpha_1\beta_1)^2} + \frac{6N_o^2 \cdot (B_2^2 - 4B_1B_2 + 7B_1^2) \cdot (\alpha_1^3\beta_3 + 2\alpha_1\alpha_2\beta_2 + \alpha_3\beta_1)^2}{(\alpha_1\beta_1)^2}. \quad (3.1.33)$$

3.1.3 Laser Model

If the quadratic term involving B_2 and B_1 in (3.1.24) is approximated by

$$B_2^2 - 4B_1B_2 + 7B_1^2 \approx (B_2 - B_1)^2, \quad (3.1.34)$$

then the resulting convolution value for the CTB will be slightly over-estimated compared to the actual value. Figure 3.1.3 shows the over-approximation ratio vs the upper bandwidth, with the lower bandwidth set at 50 MHz. The approximation ratio is the ratio of the approximation value to the actual value shown in (3.1.34) and it gets smaller as the bandwidth is increased.

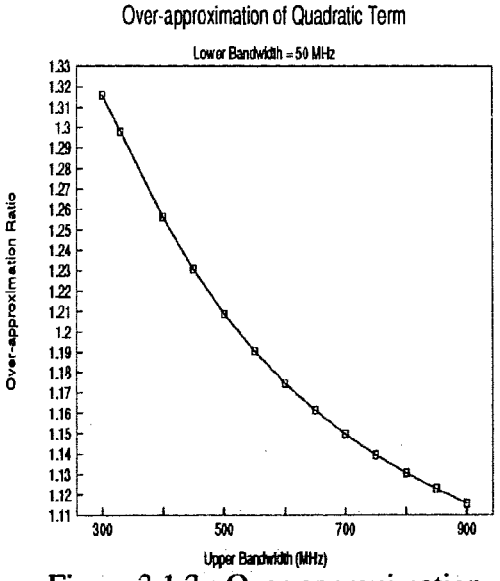

Figure 3.1.3.: Over-approximation in Quadratic Term

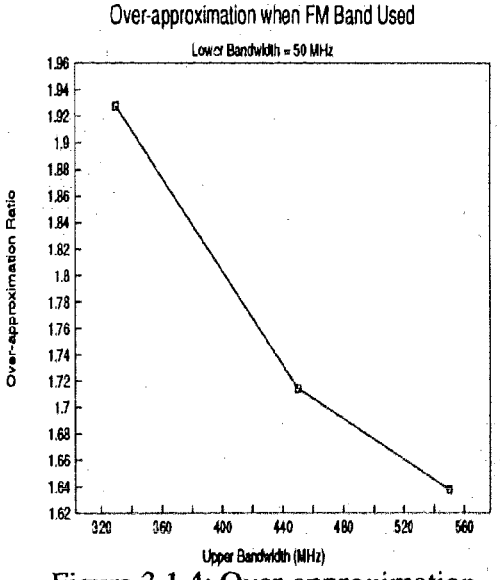

Figure 3.1.4: Over-approximation when FM Band is included

If the convolutions are performed with the frequencies in the FM band from 88 MHz to 120 MHz removed, the third order convolution values are smaller as there is less power. These convolution values were obtained numerically, and the difference between these numbers and the approximation in (3.1.34) are shown in Figure 3.1.4. Again, the difference is shown as the ratio between (3.1.34) and the simulation value. The over-approximation ranges from between 1.5 and 2 for upper bandwidths from 330 MHz to 550 MHz, which means that the CTB using the approximation will be 2 to 3 dB larger than the expected actual values.

However, the substitution results in a simplified form of (3.1.33),

$$NLD = \frac{2N_o \cdot (B_2 - B_1) \cdot (\alpha_1^2\beta_2 + \alpha_2\beta_1)^2}{(\alpha_1\beta_1)^2} + \frac{6N_o^2 \cdot (B_2 - B_1)^2 \cdot (\alpha_1^3\beta_3 + 2\alpha_1\alpha_2\beta_2 + \alpha_3\beta_1)^2}{(\alpha_1\beta_1)^2}. \tag{3.1.35}$$

If an actual CATV signal is applied at the input, the mean square signal power of a single carrier is

$$P_{carrier} = \frac{m^2}{2}, \tag{3.1.36}$$

where m is the modulation index per channel. If there are N channels, the total signal power in the laser is

$$P_{total} = \frac{m^2 \cdot N}{2}. \tag{3.1.37}$$

The total input signal power using the white noise source of the band-limited spectral density $N_o/2$ is

$$P_{Tnoise} = 2\int_{B_1}^{B_2} \frac{N_o}{2} df = N_o \cdot (B_2 - B_1). \tag{3.1.38}$$

The powers in (3.1.37) and (3.1.38) represent the total input power to the system. These powers must be the same, so (3.1.37) can be substituted for (3.1.38) to obtain (3.1.35) in terms of the modulation index and the number of channels, hence

$$NLD = \frac{2\frac{m^2 \cdot N}{2} \cdot (\alpha_1^2\beta_2 + \alpha_2\beta_1)^2 + 6\frac{m^4N^2}{4} \cdot (\alpha_1^3\beta_3 + 2\alpha_1\alpha_2\beta_2 + \alpha_3\beta_1)^2}{(\alpha_1\beta_1)^2}. \quad (3.1.39)$$

Without a predistorter, (3.1.39) reduces to (assuming $\beta_1 = 1$, $\alpha_1 = 1$, and α_2, $\alpha_3 = 0$)

$$NLD = m^2N \cdot (\beta_2)^2 + \frac{3}{2}m^4N^2 \cdot (\beta_3)^2. \quad (3.1.40)$$

From (3.1.40), the values of β_2 and β_3 can be calculated from the distortion measured with a typical CATV laser. For example, a laser with a specified CSO = -69 dBc and CTB = -73 dBc at a modulation index of .05 with 40 channels (330 MHz) results in $|\beta_2| = 0.00112$ and $|\beta_3| = 0.001828$.

If the laser coefficients (β's) are both determined to be negative, then the predistorter coefficients (α's) will be positive. Figure 3.1.5 shows a contour plot of the total non-linear distortion vs variations in α_2 and α_3 with the beta values calculated above using equation (3.1.39).

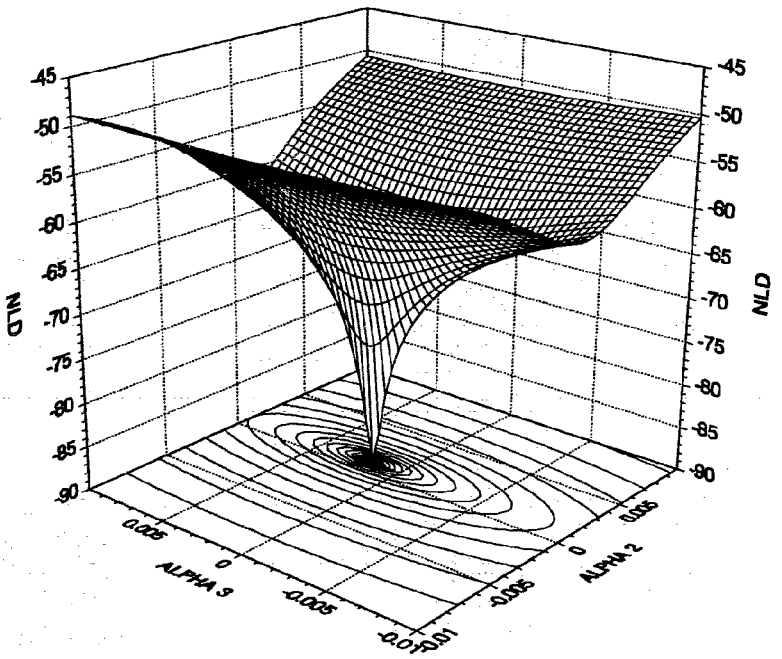

Figure 3.1.5: NLD vs Predistorter Coefficients

From Figure 3.1.5 the quadratic dependence of α_2 and α_3 on the composite distortion power can easily be seen. Thus, the predistorter coefficients can converge to the optimum values by simply measuring the NLD at the output of the laser.

3.2 Comparison with Beat Count Method

Equation (3.1.40) differs from the standard method of obtaining polynomial coefficients from published beat charts. Generally, CSO and CTB values are calculated in the following way. The second and third harmonic distortion from a single input tone are measured, and then correction factors are added. The correction factors or beat counts are based on the actual allocation of the CATV channels in the band.

For example, Daly [10] models a laser diode as a third order polynomial and calculates the CSO and CTB using the expressions

$$CSO = 2HD + 6 + 10\log(NT2)\ dBc, \tag{3.2.1}$$

$$CTB = 3HD + 15.6 + 10\log(NT3)\ dBc, \tag{3.2.2}$$

where 2HD is the measured second harmonic distortion in dBc and 3HD is the measured third harmonic distortion in dBc for a single input tone. The values of NT2 and NT3 are based on the number of channels and the channel allocation. Table 3.2.1 shows the values of NT2 and NT3 for the channel with the worst CSO and CTB respectively.

Table 3.2.1: Beat Count Chart

# of Channels	NT2	NT3
36	23	362
40	25	479
54	41	922
60	47	1166
77	64	~2000

The values of the coefficients for the third order polynomial model can be easily obtained from the 2HD and 3HD measurements. The input to the laser, $V_{in}(t)$, is a tone with amplitude m equal to the modulation index of the laser,

$$V_{in}(t) = m\sin(\omega t). \tag{3.2.3}$$

If $V_{in}(t)$ is applied as the input $V_d(t)$ in (3.1.2), then the resulting output will be

$$V_l(t) = \frac{\beta_2 m}{2} + \left(\beta_1 m + \frac{3}{4}\beta_3 m^3\right)\sin(\omega t) - \frac{\beta_2 m^2}{2}\cos(2\omega t) - \frac{\beta_3 m^3}{4}\sin(3\omega t). \tag{3.2.4}$$

Since β_3 is much smaller than β_1, the $\sin(\omega t)$ term is essentially equal to $\beta_1 m \sin(\omega t)$. The values of 2HD and 3HD in dBc are then

$$2HD = 10\log\left(\frac{\beta_2^2 m^2}{4\beta_1^2}\right) dBc, \tag{3.2.5}$$

$$3HD = 10\log\left(\frac{\beta_3^2 m^4}{16\beta_1^2}\right) dBc. \tag{3.2.6}$$

Note that both the CSO and CTB are functions of m^2 and m^4 respectively, the same relationship as in (3.1.40).

If it is assumed that a laser has coefficients $\beta_1 = 1$, $\beta_2 = -0.001$, $\beta_3 = -0.001$, then the worst case CSO and CTB can be calculated using (3.2.1) and (3.2.2). If the modulation index is m = 0.05 and there are 40 channels, the beat chart method results in CSO = -72.06 dBc and CTB = -81.67 dBc. Using the gaussian approximation, (3.1.40), CSO = -70 dBc and CTB = -78.24 dBc.

The results based on the gaussian approximation are within 2 dB for the CSO and 3.4 dB for the CTB compared to the beat chart method. The over-estimation of 3 dB in the CTB was expected due the approximation resulting from the FM band being ignored.

A simulation was performed with 40 randomly phased carriers to verify the two theoretical calculations. The simulation computed the CSO and CTB levels using the same beta values as in the calculations. The simulation was run 20 times and the results were averaged. The worst case CSO was -74 dBc and the worst case CTB was -82.6 dBc. The simulation values closely match the theoretical results.

If the number of channels is increased to 60 with the same beta values and modulation index, then the beat count method gives CSO = -69.32 dBc and CTB = -77.74 dBc. The gaussian approximation method gives CSO = -68.24 dBc and CTB = -74.72 dBc. The difference between the two methods becomes smaller as the number of channels is increased as expected from the results of Figures 3.1.3 and 3.1.4. Therefore, the gaussian approximation method provides a good analytical model for the worst case CSO and CTB, particularly for large numbers of channels. The theoretical CTB value will be slightly over-estimated, but the correct CTB level can be obtained by subtracting the over-approximation factor shown in Figure 3.1.4.

3.3 Nonlinearities and Clipping

Considerable attention has been spent by researchers to determine the fundamental limit of the distortion in a CATV Lightwave system [15-18]. This work is based on all of the distortion being produced due to signal clipping and a perfectly linear laser L-I curve. The clipping distortion is caused from the input signal level exceeding the laser's input current range. For example, 40 channels modulated at 5% per channel are capable of adding in phase to produce a total signal of modulation 2. Obviously, the input is twice as large as the laser can handle. However, when the input signals are randomly phased as CATV signals are, the average total modulation index is less than 1 and only occasionally will the phases add such that there is clipping by the laser.

An 'exact' equation for calculating the minimum distortion levels due to clipping has been proposed by Qun Shi et. al. [18]. Their equations for the CSO and CTB are shown below and are plotted for a 40 channel system along with the total non-linear distortion (NLD) (the sum of the CSO and CTB) versus the modulation index in Figure 3.3.1.

$$CSO = \frac{K_{2v}}{8\pi N} e^{-\frac{2}{m^2 N}} \frac{1+erf\left(\frac{1}{m\sqrt{N}}\right)}{2} \tag{3.3.1}$$

$$CTB = \frac{K_{3v}}{16\pi N^3} m^{-2} e^{-\frac{2}{m^2 N}} \frac{1+erf\left(\frac{1}{m\sqrt{N}}\right)}{2} \tag{3.3.2}$$

The values of K_{2v} and K_{3v} are the NT2 and NT3 values from the beat chart for a given number of channels, N. For 40 channels, $K_{2v} = 25$ and $K_{3v} = 479$.

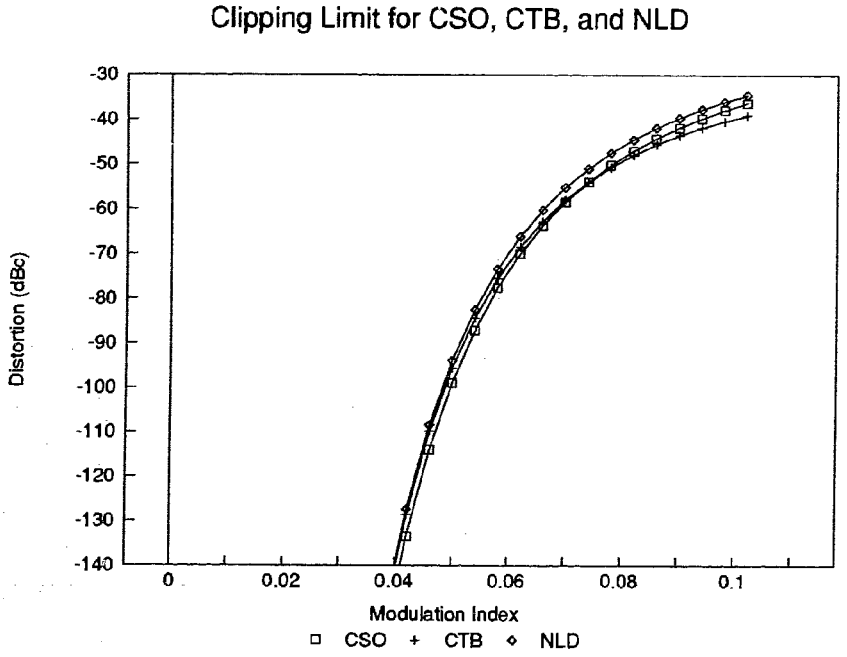

Figure 3.3.1: Clipping Limit for CSO, CTB, and NLD

Experiments have been performed to verify the results of the clipping model [16,19]. Chung and Jacobs [19] measured the NLD vs the modulation index for a 42 channel CATV system. Their results are plotted vs the clipping model in Figure 3.3.2.

From Figure 3.3.2, it is apparent that Chung and Jacobs' experimental results closely match the clipping limit for modulation indices above about 0.06 per channel. Below 0.06, the NLD drops slowly as the modulation index is reduced. This variance from the clipping model was attributed by Chung and Jacobs to the intrinsic non-linearities of the laser [19].

Chung and Jacobs measured the CSO and CTB down to m=0.042. At this point CSO ≈ -69 dBc and CTB ≈ -73 dBc [19]. If these values are worked back to the polynomial model of equation (3.1.40), then the resulting coefficients are $\beta_2 = 0.0013$ and $\beta_3 = 0.0034$. Equation (3.1.40) is also plotted in Figure 3.3.2 using these beta values.

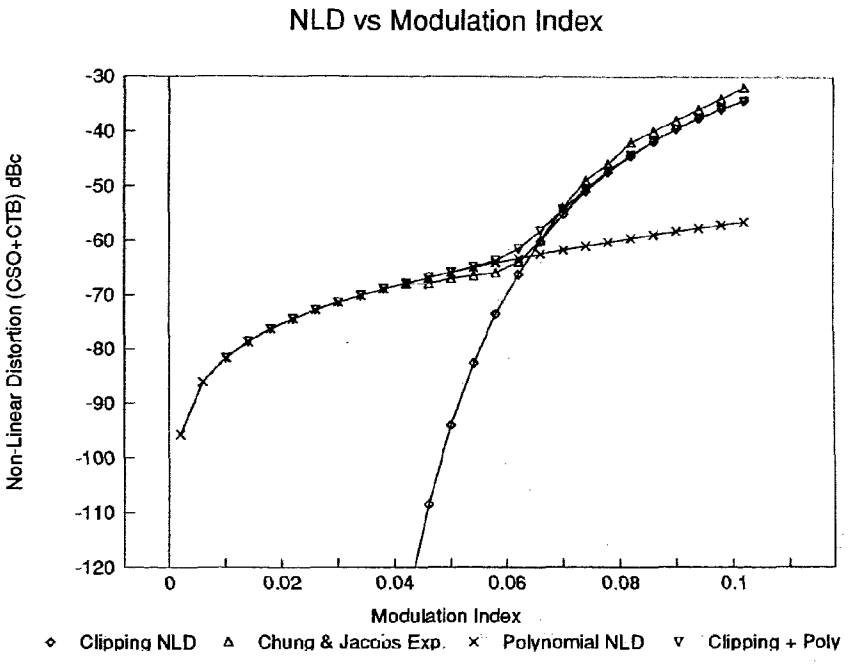

Figure 3.3.2: NLD vs Modulation Index

It is apparent that the polynomial model closely matches the experimental results of Chung and Jacobs for low modulation indices. Since most commercial CATV systems operate at modulation indices around 0.04 to 0.05 per channel, the NLD or CSO and CTB of the laser diode could be reduced using a third order predistorter to the point where the fourth and higher order non-linearities dominate. A perfect predistorter of n^{th} order could technically achieve the fundamental clipping limit.

From Figure 3.3.2, the polynomial model is valid only for modulation indices where the NLD from the laser non-linearities is higher than the NLD caused by clipping. To provide a more accurate model of the laser, the polynomial model and the clipping model were combined and this curve is also shown in Figure 3.3.2.

3.4 Predistortion

By adding a predistorter to linearize the laser, the NLD of the laser can be reduced. If the predistorter is to be constructed from discrete diodes, then the second

and third order coefficients will have some dependence on one another. However, it is possible to design the coefficient circuitry so that the coefficient dependence is negligible and the second and third order coefficients can be varied independently.

Figures 3.4.1 and 3.4.2 show the variation of the CSO and CTB levels vs the predistorter coefficient using the laser beta values of -0.0013 and -0.0024 for β_2, and β_3 respectively. In each figure, the results are shown for modulation indices of .05 and .055. The fundamental clipping limits for these modulation indices are also shown. The figures show that the CSO and CTB levels vary quadratically with the predistorter coefficients. Also, the figures show that for m=0.055, predistortion can only achieve the clipping distortion level. However, reduction of over 20 dB for both the CSO and CTB is possible at m=0.05.

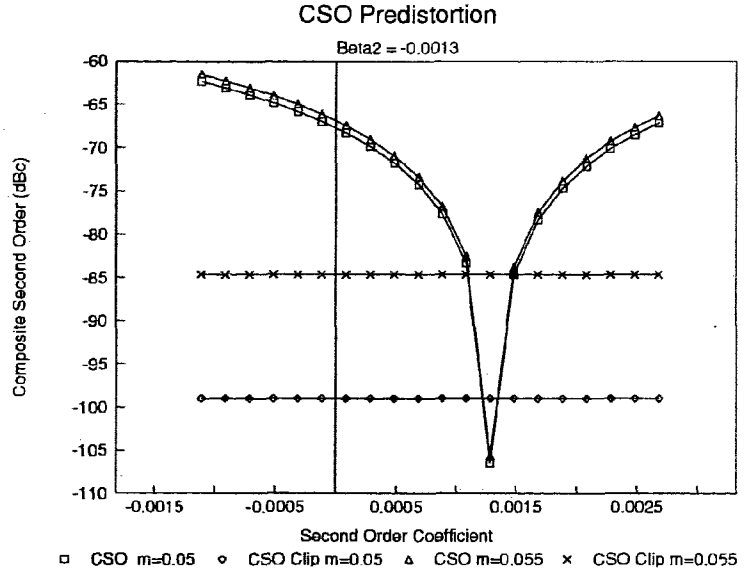

Figure 3.4.1: CSO Predistortion

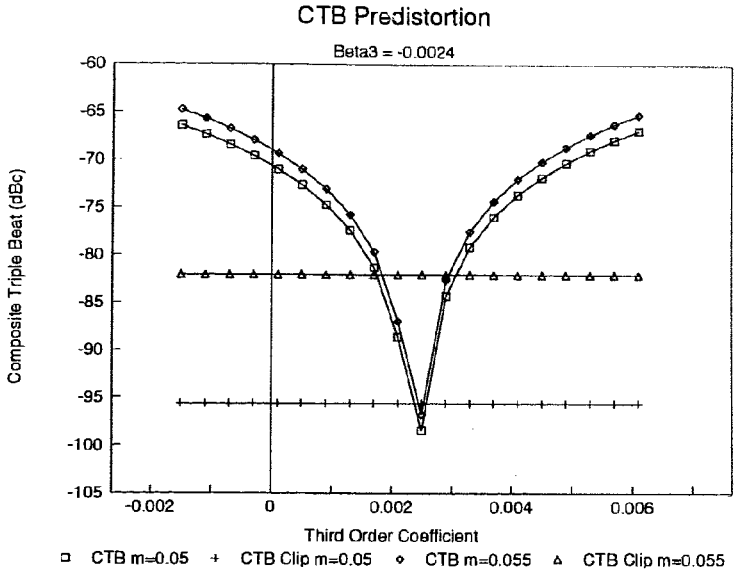

Figure 3.4.2: CTB Predistortion

Figure 3.4.3 shows the total NLD with and without the predistorter for a variety of predistorter coefficients using the laser beta values above. It is clear that for this laser, the CSO dominates over the CTB since the NLD is lower when only the CSO is cancelled ($\alpha_2 = 0.0013, \quad \alpha_3 = 0$) compared to when only the CTB is cancelled ($\alpha_2 = 0, \quad \alpha_3 = 0.0024$). As the coefficients are adjusted more closely to the optimum ($\alpha_2 = 0.001, \quad \alpha_3 = 0.001$) and ($\alpha_2 = 0.0012, \quad \alpha_3 = 0.002$), the NLD levels approach the clipping limit. It is important to note, however, that the CSO and CTB may not achieve the clipping limit, even with the correct predistorter coefficients due to higher order non-linearities that are not being cancelled by the third order predistorter.

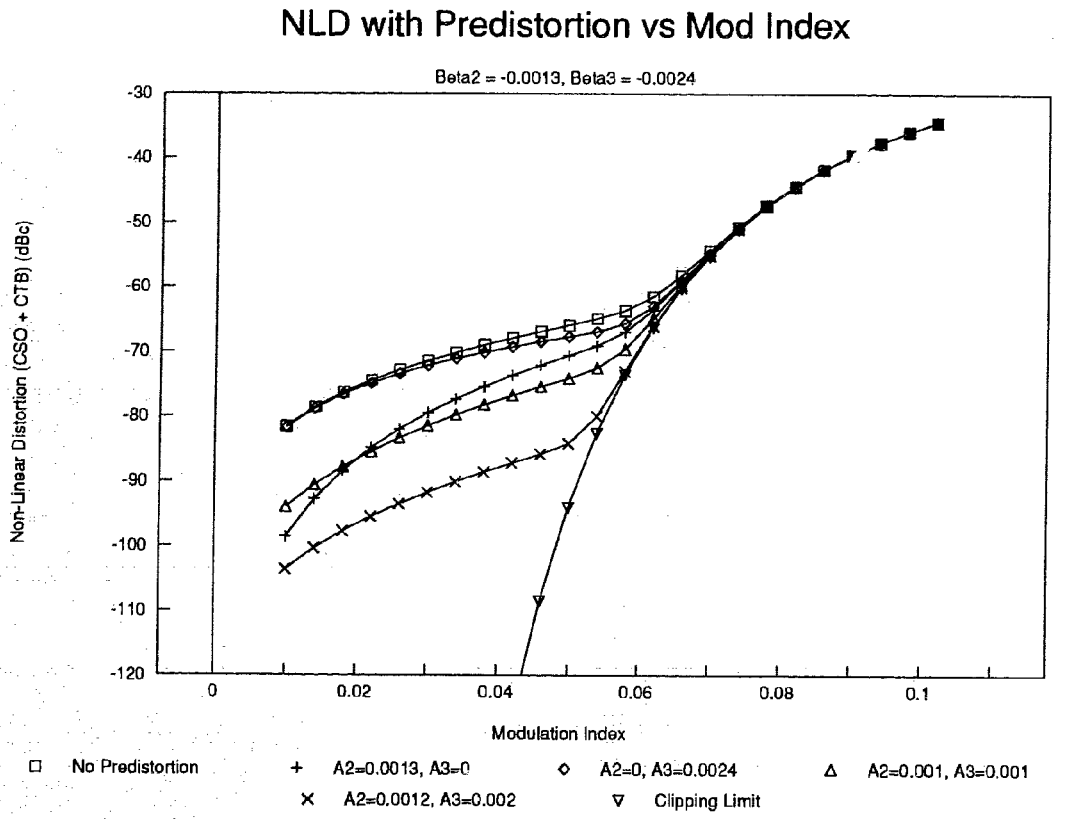

Figure 3.4.3: NLD vs Modulation Index for Various Predistorter Coefficients

These results indicate that predistortion is capable of reducing the CSO and CTB produced by the laser at modulation indices used by the CATV industry. Also, the third order polynomial model appears to correlate well with already published data. In the next section some theory about predistortion is presented.

4 PREDISTORTER THEORY

The analysis of Section 3 is based on the assumption that a laser diode can be modelled as a third order polynomial. The predistorter is also modelled as a third order polynomial but with opposite coefficients. The predistorter is required to generate second and third order distortion independently so that the levels of the distortion (coefficients) can be varied. This section explains how the predistorter generates the second and third order distortion, and how much reduction one can expect from imbalances between the predistorter and the laser.

4.1 Harmonic Generation using Discrete Diodes

The harmonic generators (second and third order distortion generators) were constructed using discrete Schottky diodes. By arranging the diodes in certain configurations, it was possible to generate the second or third harmonic independently. A mathematical derivation of the harmonic generator operation will now be shown.

The equation for a diode is

$$I = I_s\left(e^{\frac{V}{nV_T}} - 1\right), \tag{4.1.1}$$

where V is the voltage across the diode measured from the anode to the cathode, V_T = 25 mV, and n is a constant which is device dependent.

The diode equation for $V >> nV_T$ can be approximated to

$$I \approx I_s e^{\frac{V}{nV_T}}. \tag{4.1.2}$$

The term e^x can be expanded into a series as

$$e^x = 1 + x + \frac{x^2}{2!} + \frac{x^3}{3!} + \frac{x^4}{4!} + \frac{x^5}{5!} + \ldots \tag{4.1.3}$$

Therefore, I can be expressed as

$$I = I_s + \frac{I_s V}{nV_T} + \frac{I_s}{2!}\left(\frac{V}{nV_T}\right)^2 + \frac{I_s}{3!}\left(\frac{V}{nV_T}\right)^3 + \ldots \tag{4.1.4}$$

For the second harmonic generator, two diodes can be arranged so that the even terms of the series expansion add together and the odd terms cancel. Figure 4.1.1 shows a diagram of the second harmonic generator.

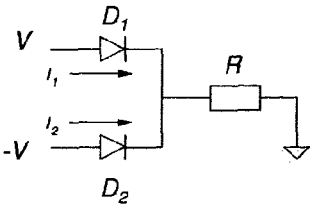

Figure 4.1.1: Second Harmonic Generator

Two forward biased diodes are used, each with identical bias currents I_1 and I_2. A small AC signal V is applied on top of the bias current to diode D_1 and the signal -V is applied on top of the bias current to diode D_2. The output AC voltage across the resistor R can be determined using superposition. The output from diode D_1 will be

$$V_{D1} = R\left(I_s + \frac{I_s V}{nV_T} + \frac{I_s}{2!}\left(\frac{V}{nV_T}\right)^2 + \frac{I_s}{3!}\left(\frac{V}{nV_T}\right)^3 + \ldots\right), \tag{4.1.5}$$

and the output from diode D_2 will be

$$V_{D2} = R\left(I_s - \frac{I_s V}{nV_T} + \frac{I_s}{2!}\left(\frac{V}{nV_T}\right)^2 - \frac{I_s}{3!}\left(\frac{V}{nV_T}\right)^3 + \ldots - \ldots\right). \tag{4.1.6}$$

Thus, V_o is equal to

$$V_o = V_{D1} + V_{D2}, \tag{4.1.7}$$

$$V_o = 2R\left(I_s + \frac{I_s}{2!}\left(\frac{V}{nV_T}\right)^2 + even\ powers\right), \tag{4.1.8}$$

which is a function only of V^2 and the higher order even terms. If it is assumed that the fourth and higher order terms are negligible compared to the second order term (V is small) then the output signal will consist almost entirely of the second harmonic. The DC portion of the output can be eliminated using coupling capacitors.

For the third harmonic generator, two diodes are arranged in an anti-parallel configuration as shown in Figure 4.1.2.

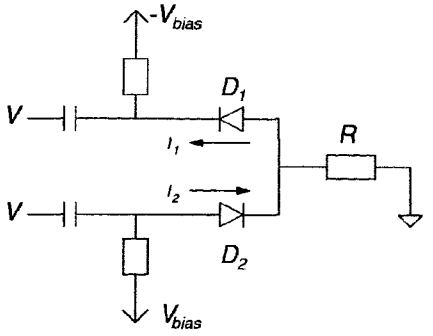

Figure 4.1.2: Third Harmonic Generator

Each diode is forward biased with equal bias currents flowing from the anode to the cathode. An input AC voltage V is applied on top of the bias currents and the AC output voltage can be determined from the current flowing through the resistor R using superposition.

The output voltage from diode D_2 is

$$V_{D2} = R\left(I_s + \frac{I_s V}{nV_T} + \frac{I_s}{2!}\left(\frac{V}{nV_T}\right)^2 + \frac{I_s}{3!}\left(\frac{V}{nV_T}\right)^3 + \ldots\right). \tag{4.1.9}$$

Since the bias current flowing through D_1 is in the opposite direction to the input voltage V, the AC current level flowing through D_1 is equivalent to that caused by an input voltage of -V. Thus, the current I_1 is equal to

$$I_{D1} = I_s - \frac{I_s V}{nV_T} + \frac{I_s}{2!}\left(\frac{V}{nV_T}\right)^2 - \frac{I_s}{3!}\left(\frac{V}{nV_T}\right)^3 + \ldots - \ldots \tag{4.1.10}$$

where the current I_1 is flowing in the opposite direction to the current I_2. The output voltage across R will be

$$V_o = V_{D2} - I_{D1}R. \tag{4.1.11}$$

The signs of the terms for I_1 in (4.1.10) will flip, and the output voltage will be

$$V_o = 2R\left(\frac{I_s V}{nV_T} + \frac{I_s}{3!}\left(\frac{V}{nV_T}\right)^3 + odd\ powers\right). \tag{4.1.12}$$

The third harmonic generator actually generates the fundamental, third, fifth, and higher odd order terms. The fundamental term that is generated by this circuit is not wanted, but provided that its power level is well below the input fundamental power required for the non-linear device, it won't have much effect. The fifth and higher order terms are assumed to be negligible compared to the third order term (V is small) so the output will consist only of the fundamental and third harmonic.

From this derivation, it is easy to see that for a single forward biased diode with the input signal applied to the anode, the current as a function of the input voltage is

$$I_{for} = aV + bV^2 + cV^3 + \ldots \tag{4.1.13}$$

For a forward biased diode with the input applied to the cathode, which we will call a "reverse diode", the current as a function of the input voltage is

$$I_{rev} = aV - bV^2 + cV^3 - \ldots + \ldots \tag{4.1.14}$$

In CATV applications, the laser diode is biased as a "reverse diode" using the above definition. Therefore, its expected characteristic will be the same as equation (4.1.14) above.

The form of the polynomial equations in (4.1.13) and (4.1.14) do not contain the absolute value signs around the third order term as in (3.1.1). Provided that the input signals are real, both equations will produce identical results and are therefore equivalent.

4.2 Coefficient Amplitude and Phase Considerations

The power of the second and third order distortion depends only on the magnitude of the second and third order polynomial coefficients; the sign of the coefficients are irrelevant. However, the sign of the polynomial coefficients need to be known so that

the predistorter can be built with coefficients of the opposite sign. The magnitude and sign of the coefficients can be determined from the amplitude and phase of the second and third order harmonics.

For example, assume a laser diode has the I-V (L-I) relationship

$$I = aV - bV^2 + cV\,|\,V\,|^2, \tag{4.2.1}$$

where a, b, and c are real coefficients.

If the input voltage V is a real sinusoid, $V = A\sin(\omega t + \theta)$, then the output, I, will be

$$\begin{aligned} I &= aA\sin(\omega t+\theta) - b(A\sin(\omega t+\theta))^2 \\ &\quad + c(A\sin(\omega t+\theta)\,|\,A\sin(\omega t+\theta)\,|^2), \end{aligned} \tag{4.2.2}$$

$$\begin{aligned} I &= aA\sin(\omega t+\theta) - \frac{bA^2}{2}(1-\cos(2\omega t+2\theta)) \\ &\quad + cA^3\left(\frac{3}{4}\sin(\omega t+\theta) - \frac{1}{4}\sin(3\omega t+3\theta)\right). \end{aligned} \tag{4.2.3}$$

Equation (4.2.3) can be expanded to find the phase and amplitude of each harmonic.

$$DC\,term = -b\frac{A^2}{2}. \tag{4.2.4}$$

$$Fund = \left(aA + \frac{3}{4}cA^3\right)\sin(\omega t+\theta), \tag{4.2.5}$$

$$2^{nd} = b\frac{A^2}{2}\cos(2\omega t+2\theta) = b\frac{A^2}{2}\sin(2\omega t+2\theta+90°), \tag{4.2.6}$$

$$3^{rd} = -c\frac{A^3}{4}\sin(3\omega t+3\theta) = c\frac{A^3}{4}\sin(3\omega t+3\theta+180°), \tag{4.2.7}$$

Equations (4.2.4) to (4.2.6) show that if the input signal has a phase shift $\theta = 0$, then the second harmonic will have a +90° phase shift and the third harmonic will have

a 180° phase shift. This means that the predistorter must produce a second harmonic with a -90° phase shift and a third harmonic with a 0° phase shift. This will occur if the polynomial signs are reversed for the second and third coefficients.

To obtain perfect cancellation, the magnitude of the predistorter harmonics must be exactly the same as the magnitude of the non-linear device and the phase of the predistorter must be exactly 180° out of phase with the non-linear device. If there is some magnitude and phase imbalance, then the amount of cancellation will vary.

As a simple example, suppose that the predistorter and the laser are both second order polynomials with coefficients a, b, and x, y respectively.

$$V_{predist} = aV_{in} - bV_{in}^2, \tag{4.2.8}$$

$$V_{laser} = xV_{predist} + yV_{predist}^2. \tag{4.2.9}$$

Using the input signal $V_{in} = A\sin(\omega t + \theta)$ results in the predistorter output being

$$V_{predist} = aA\sin(\omega t + \theta) + b\frac{A^2}{2}\sin(2\omega t + 2\theta + 90°), \tag{4.2.10}$$

excluding the DC term. The laser output is then equal to

$$\begin{aligned} V_{laser} = {} & xaA\sin(\omega t + \theta) + xb\frac{A^2}{2}\sin(2\omega t + 2\theta + 90°) \\ & + y(a^2A^2\sin^2(\omega t + \theta) + abA^3\sin(\omega t + \theta)\sin(2\omega t + 2\theta + 90°) \\ & + b^2\frac{A^4}{4}\sin^2(2\omega t + 2\theta + 90°)). \end{aligned} \tag{4.2.11}$$

Expanding (4.2.11), the result excluding DC terms is

$$V_{laser} = xaA\sin(\omega t+\theta)+xb\frac{A^2}{2}\sin(2\omega t+2\theta+90°) \quad (4.2.12)$$

$$-ya^2\frac{A^2}{2}\sin(2\omega t+2\theta+90°)$$

$$+yab\frac{A^3}{2}(\cos(\omega t+\theta+90°)-\cos(3\omega t+3\theta+90°))$$

$$+yb^2\frac{A^4}{8}\cos(4\omega t+4\theta+180°)).$$

If a = x = 1, and |b| = |y|, then the second order terms will cancel each other. Note that there are additional interfering terms resulting from the cascade of the predistorter and the laser. These terms occur at the fundamental frequency, the third harmonic, and the fourth harmonic. However, these terms are all very much smaller than the fundamental and second order terms and therefore can be ignored. Thus, only the first three terms of (4.2.12) remain.

The two second order terms of (4.2.12) will cancel each other completely if they are exactly equal in amplitude and opposite in phase. Any amplitude or phase imbalance will result in incomplete cancellation. If incomplete cancellation occurs due to a phase imbalance, then it means that the composite polynomial coefficients have a complex component.

To show the effect of amplitude and phase imbalance, denote the two second order terms of (4.2.12) as V_1 and V_2;

$$V_1 = V_a\cos(\omega t), \quad (4.2.13)$$

$$V_2 = V_b\cos(\omega t+(\theta+180°)), \quad (4.2.14)$$

where V_a and V_b are the amplitudes of the signals and θ is the phase imbalance. In the predistortion operation, these two signals are added together. If the two signals V_1 and V_2 are treated as vectors during addition, their x and y components will be

$$
\begin{aligned}
V_{1x} &= V_a, \\
V_{1y} &= 0, \\
V_{2x} &= -V_b \cos(\theta), \\
V_{2y} &= -V_b \sin(\theta).
\end{aligned}
\tag{4.2.15}
$$

The resultant vector V_3 will have components

$$
\begin{aligned}
V_{3x} &= V_a - V_b \cos(\theta), \\
V_{3y} &= -V_b \sin(\theta),
\end{aligned}
\tag{4.2.16}
$$

and the magnitude and phase will be

$$|V_3| = \sqrt{V_a^2 - 2V_a V_b \cos(\theta) + V_b^2}, \tag{4.2.17}$$

$$\angle V_3 = arctan\left(\frac{V_a - V_b \cos(\theta)}{-V_b \sin(\theta)}\right). \tag{4.2.18}$$

Figures 4.2.1 and 4.2.2 show plots of the output magnitude and phase when the input signals have identical amplitudes and a given phase imbalance.

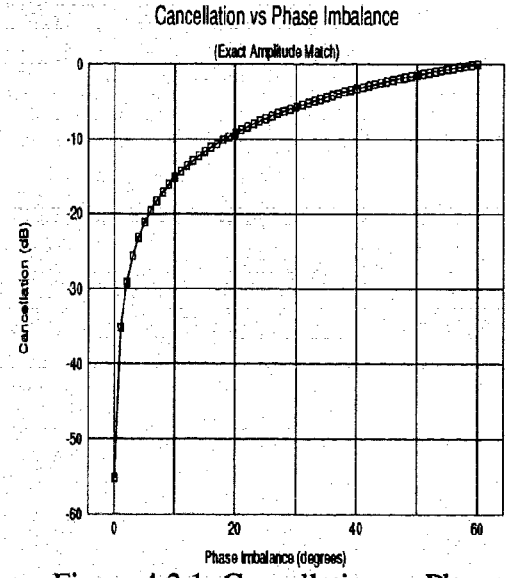

Figure 4.2.1: Cancellation vs Phase Imbalance

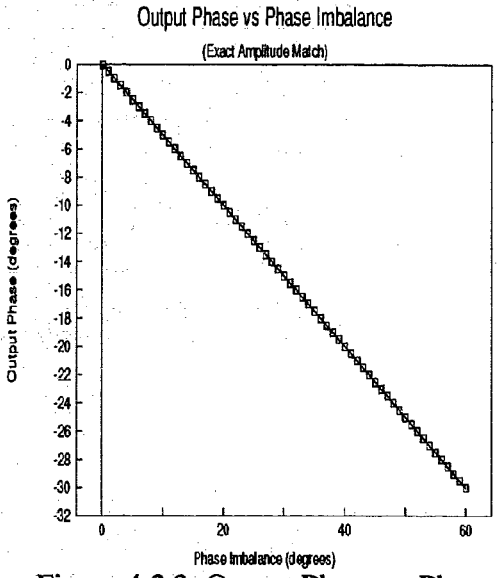

Figure 4.2.2: Output Phase vs Phase Imbalance

Figures 4.2.3 and 4.2.4 show plots of the output magnitude and phase when the input signals have a constant phase error of 3° and the voltage V_a is fixed while V_b is varied.

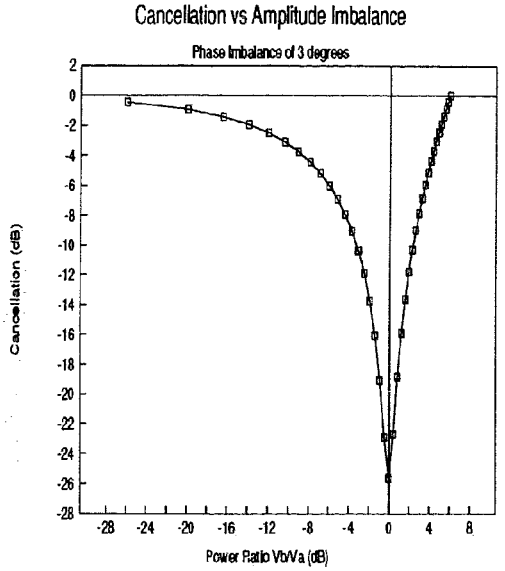

Figure 4.2.3: Cancellation vs Amplitude Imbalance

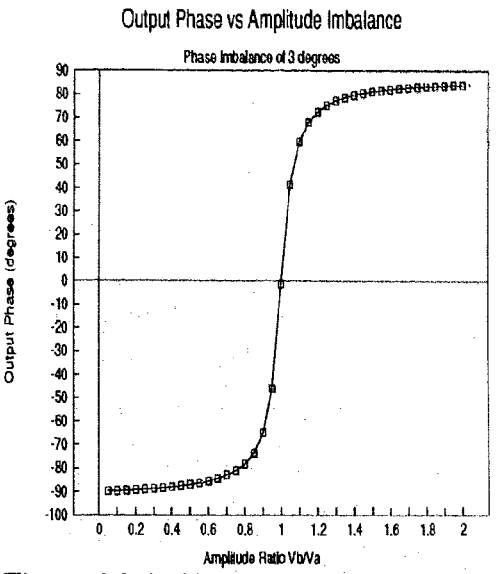

Figure 4.2.4: Output Phase vs Amplitude Imbalance

Figures 4.2.1 to 4.2.4 show that both the amount of cancellation and the output phase after cancellation are highly sensitive to amplitude and phase imbalances. Phase imbalances of more than 10° considerably reduce the amount of cancellation possible. Since the predistorter is to be constructed from discrete diodes, there will likely be some phase imbalance between the fundamental signal and the harmonics due to parasitic capacitance and inductance involved with the diode and surrounding circuitry. However, provided the phase imbalance is no greater than 20 degrees, cancellation of up to 10 dB can still be achieved provided the amplitude is balanced.

The predistorter amplitude dependence also shows that cancellation is more sensitive to output powers from the predistorter that are too large as opposed to output powers that are too small. However, the maximum cancellation point is well defined and can easily be found adaptively.

5 SYSTEM DESIGN

The design procedure for the predistorter incorporated five basic steps. They were: (1) characterize the laser, (2) determine the optimum predistorter, (3) construct the predistorter, (4) test the predistorter, and (5) predistort the laser. These steps are outlined in more detail in the sections to follow.

In order to characterize the laser and the predistorter polynomial coefficients, the phase of the harmonic signals of both the laser and the predistorter must be measured. The phase information is required because it determines the sign of the coefficients. The measurement technique used to measure the phase of the harmonic signals is described below.

5.1 Relative Phase Measurement

From Section 4.2, the sign of the polynomial coefficients determines the phase of the harmonic signals, and the magnitude of the polynomial coefficients determines the amplitude of the harmonic signals. Since the sign of the coefficients is often not known in advance, the amplitude and phase of the harmonic signals must be measured to determine the corresponding coefficient magnitude and sign.

The magnitude of the coefficients can be easily determined by measuring the power of the harmonics. However, the sign must be determined from phase measurements. The phase measurements were made relative to the input fundamental signal and the technique is as follows.

To measure the phases of the output fundamental and harmonics relative to the input fundamental signal, the test setup in Figure 5.1.1 was used. Two signal generators were phase-locked to each other, with one of the signal generators, generator 1, providing the fundamental input signal for the diode and the other signal generator, generator 2, set to the frequency of the output signal to be measured. A filter was added to the generator 1 output to suppress any harmonics coming from the source. A variable phase shifter was connected to generator 2, and the generator 2 signal was added to the output of the diode using a passive power summer.

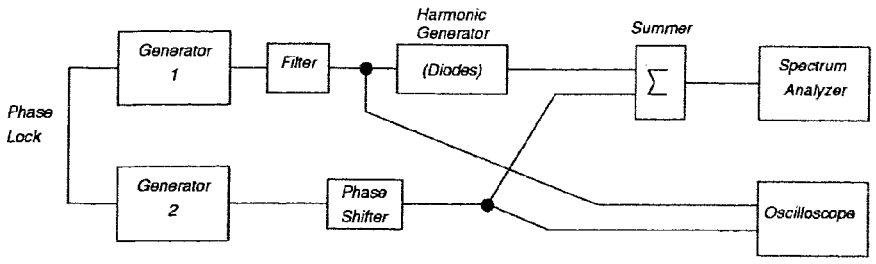

Figure 5.1.1: Phase Measurement Setup

The amplitude of the generator 2 frequency was set to the same level as the amplitude of the diode output frequency being measured using the power control knob on generator 2. The power summer output was connected to a spectrum analyzer so that the power of the harmonic to be measured could be seen. The phase of the generator 2 signal was then varied using the variable phase shifter so that the generator 2 signal cancelled the output signal from the diode. The cancellation was easily seen on the spectrum analyzer as a reduction in power. When full cancellation had been achieved, it meant that the phase of the generator 2 output was exactly 180° out of phase with the phase of the diode output.

Then, the generator 2 output and the generator 1 input were connected to a high frequency oscilloscope and the phase difference between the generator 1 signal (input fundamental sine wave) and the generator 2 signal (output fundamental or harmonic sine wave) was measured using the fundamental sine wave axis as a reference. The generator 2 signal was inverted 180° using the invert switch on the oscilloscope to compensate for the 180° phase shift used to obtain the cancellation. (Cancellation of the signal provides a much more accurate phase measurement than power addition since the cancellation is very sensitive to the phase as shown in Figure 4.2.1).

The above phase measurements are all in degrees relative to the input fundamental signal, using the input fundamental signal axis as a reference. The input fundamental signal goes through one complete cycle in 360°. The second harmonic signal goes through two complete cycles or 720° when the fundamental signal goes through one. This means that the second harmonic signal goes through a 360° cycle in a 180° segment of the fundamental signal. Therefore, since the second harmonic phase

shift is measured in degrees relative to the fundamental axis, the second harmonic phase shift in degrees relative to a second harmonic signal is twice the measured result. Similarly, the third harmonic phase shift relative to a third harmonic signal in degrees is three times the measured result. The input fundamental and the second and third harmonic reference signals have phase shifts of 0°.

The measured harmonic phases that have been multiplied by the appropriate factors to obtain their 'actual' values should correspond with the phases of equations (4.2.5), (4.2.6), and (4.2.7), where the value of θ is the measured phase difference between the input fundamental and the output fundamental. In equation (4.2.5), the input and output fundamental phase shifts are identical because there is no phase delay through the diode. To match the equations, the phase delay through the diode or non-linear device is being converted to a corresponding phase shift incident on the diode. However, it is clear that if the measured output phases correspond to equations (4.2.5) to (4.2.7), the sign of the coefficients is obvious.

However, a simple way of determining the sign of the coefficients from the initial measurements relative to the input fundamental exists. If the difference between the measured second harmonic phase relative to the input fundamental and the measured output fundamental phase relative to the input fundamental is -45°, then the second order coefficient is positive. If the difference is +45°, then the second order coefficient is negative. Note that twice this value will give a second harmonic phase of either +90° or -90° in degrees relative to the second harmonic, which matches the constant phase shift value in (4.2.6), depending on the sign of the second order coefficient. Similarly, if the difference between the measured third harmonic phase relative to the input fundamental and the measured output fundamental phase relative to the input fundamental is -60°, then the third order coefficient is positive, and if the difference is 0°, then the third order coefficient is negative.

Since the difference in the phase values relative to the input fundamental as explained above are easy to obtain and interpret, they are used throughout the remainder of this document.

It is important to note that this phase measurement technique had a significant amount of error involved in it. The cancellation procedure using the spectrum analyzer provided a phase accuracy of within ± 6° if the cancellation was more than 20 dB. This part of the measurement was quite accurate, but the phase reading obtained from the oscilloscope had significantly more error. Typically, the oscilloscope measurement had a reading error of about ± 6°. This error value was not bad for the output fundamental measurement, but for the second harmonic the actual phase (not the relative phase) was twice the error value and for the third harmonic the actual phase was three times the error value. However, the relative values, even with the errors, gave a good indication of the phase characteristics.

This method was used to measure the phase shifts of both the laser and the predistorter output signals. Since the predistorter harmonics must be 180° out of phase with the laser harmonics, the laser phase results must be flipped 180° to obtain the necessary predistorter phases. To avoid these calculations, the input signal levels and phases needed to predistort the laser can be measured directly using the setup shown in Figure 5.1.2.

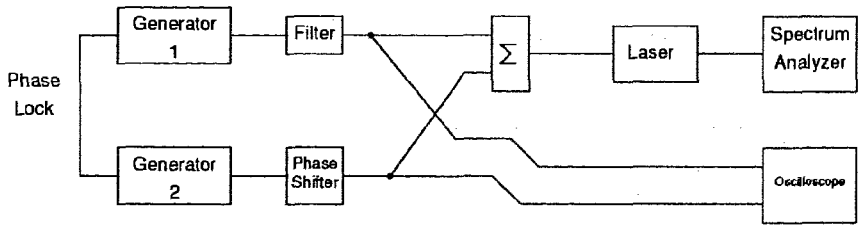

Figure 5.1.2: Laser Input Phase Measurement Technique

The setup is almost identical to that in Figure 5.1.1, except that the generator 2 signal is applied to the input of the laser, rather than at the output. In this test, the generator 2 signal is set to either the second or third harmonic frequency, and its power and phase levels are adjusted to cancel the second or third harmonic seen at the output of the laser. Then, the relative phase between the input fundamental and the input second or third harmonic is measured on the oscilloscope in degrees relative to the

input fundamental. The phase shift of the fundamental signal in this configuration will always be 0°, so with this information and the measurement, all the necessary phase calculations explained previously are still valid.

If the laser has a negative second order polynomial coefficient, then the input phase measurement would result in a relative second harmonic phase of -45° using the setup of Figure 5.1.2. If the test setup shown in Figure 5.1.1 was used, the measured phase would be +45° relative to the fundamental. Both of these phase measurement techniques were used throughout the duration of the project.

5.2 Laser Characterization

Before attempting to predistort the laser, the laser was characterized to determine its non-linear characteristics. The laser was part of an optical link that was donated by Photon Systems Corp. [20]. A block diagram of the optical link is shown in Figure 5.2.1. The laser was a Mitsubishi FU-45SDH-33 1310 nm DFB Laser diode with a fibre pigtail. The fibre was 10 km of Corning SMF-28 single mode fibre, and the optical receiver was an Ortel 2610B photodiode module. Motorola CATV hybrid amplifiers were used to amplify the input signals to the laser and the output signals from the photodiode module.

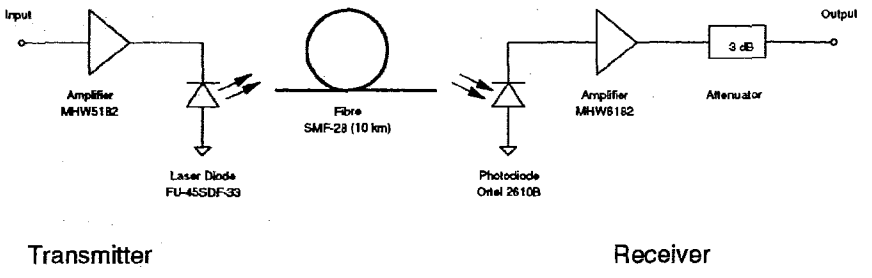

Figure 5.2.1: Optical Link

The output of the laser diode is an optical signal, hence, special optical test equipment is required in order to measure the laser's characteristics directly. Optical

test equipment was not available for this project, so the laser diode was tested by measuring the electrical signals at the output of the complete optical link. Therefore, all laser measurements were a function of the complete optical link. To ensure that the laser was the limiting factor when making the measurements, the input signals were kept small enough so that the PIN diode and associated amplifiers did not increase the distortion levels. This could be verified by measuring the distortion at different optical losses.

Two measurements were performed to characterize the laser, one to determine the modulation index, and the other to determine the laser's non-linear characteristics (polynomial coefficients).

5.2.1 Modulation Index

The modulation index at which the laser is operating needs to be known so that the laser will not be operating in the clipping region when multiple channels are provided at the input. A given operating modulation index, m, for the laser relates to a certain input power level for each input signal. For the given optical link, the required input power to achieve a certain modulation index is shown below.

The input RMS RF current to the laser for a given modulation index m is

$$i_{laserRMS} = m(I_b - I_{th})\frac{\sqrt{2}}{2} \quad A, \tag{5.2.1}$$

where I_b is the laser DC bias point current and I_{th} is the laser threshold current. The input power into the laser for the 75 ohm system is then

$$P_{\text{in laser}} = i^2_{laserRMS}(75) \quad Watts. \tag{5.2.2}$$

The input power to the system before the input amplifier is therefore

$$P_{\text{in source}} = 10\log(P_{\text{in laser}}) - G_{amp}(dB) + 30dB \quad dBm. \tag{5.2.3}$$

The corresponding RMS output current at the photodiode will be

$$i_{pRMS} = mRP\frac{\sqrt{2}}{2} \quad A, \tag{5.2.4}$$

where R is the photodiode responsivity and P is the incident average optical power from the laser. Thus, the output power from the receiver is

$$P_{outRMS} = 10\log(i_{pRMS}^2 \cdot 75) + 6dB + G_{amp}(dB) - Atten(dB) + 30dB \quad dBm, \tag{5.2.5}$$

where the 6 dB term is from the current gain in the photodiode module.

Figures 5.2.2 to 5.2.4 show the measured and calculated input and output powers for a single tone connected to the laser for three different laser bias currents, I_b. For the theoretical values, the input and output amplifiers both had a gain of 18 dB, and the output attenuator was 3 dB. The laser threshold current was 19.2 mA. The laser output optical power, P_l, and the receiver input optical power, P_{pd}, are shown and were also used in the calculation. The optical power was measured using a Tektronix TFC 200 optical power meter.

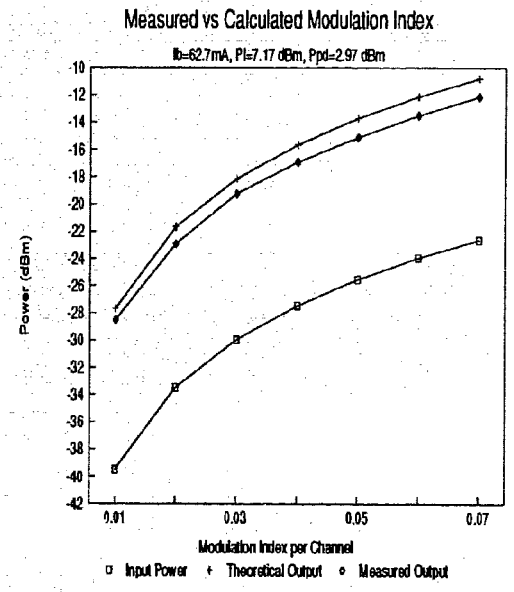

Figure 5.2.2: Modulation Index Measured Results vs Calculated Results I_b=62.7mA, P_l=7.17 dBm, P_{pd}=2.97 dBm

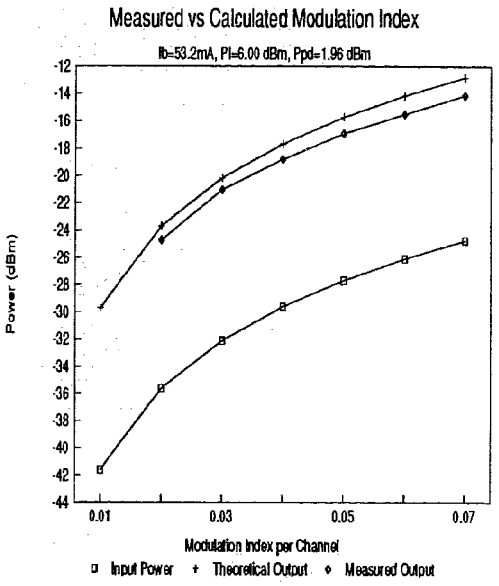

Figure 5.2.3: Modulation Index Measured Results vs Calculated Results I_b=53.2mA, P_l=6.0 dBm, P_{pd}=1.96 dBm

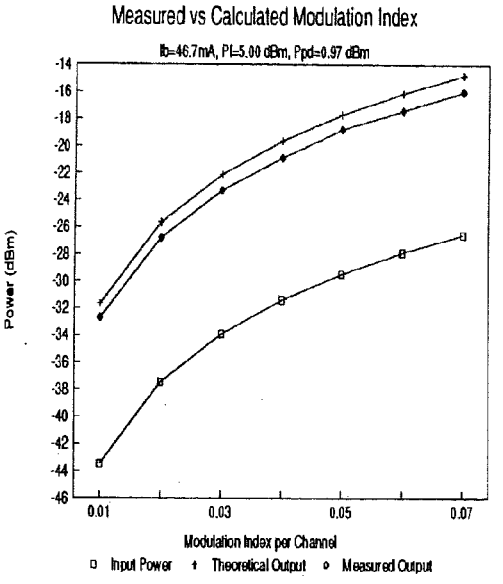

Figure 5.2.4: Modulation Index
Measured Results vs Calculated Results
I_b=46.7mA, P_i=5.0 dBm, P_{pd}=0.97 dBm

The measured and calculated input and output powers for various modulation indices and bias currents are very close. There is a systematic error of about 1 dB between the measured and calculated results, which may be due to the amplifiers providing slightly less gain than specified. However, the results show the appropriate input signal required for a given modulation index.

5.2.2 Coefficient Determination

The laser's non-linear characteristics (polynomial coefficients) were determined by measuring the amplitude and phase of the second and third harmonics for a single input tone. The phase of the harmonics was measured using the technique that results in the input phase required to predistort the laser as described in Section 5.1. The actual phase of the harmonics that the laser produced could be determined by adding 180° to the measured phase values.

The harmonics were measured with two different input powers at various frequencies. The input powers were -20 dBm and -25 dBm, which corresponded to modulation indices of about .12 and .07, respectively. These higher modulation indices were used because the harmonics were easier to measure. At low modulation indices, the harmonics were too small to make phase measurements with accuracy. However, once the phase had been determined at a higher modulation index, the phase changed little when the modulation index was lowered.

Figures 5.2.5 to 5.2.8 show the measured results of the output harmonic power levels and the input phase required to predistort the laser for input powers of -20 dBm and -25 dBm respectively. The input phase shown is the relative phase between the input second or third harmonic and the input fundamental in degrees relative to the fundamental.

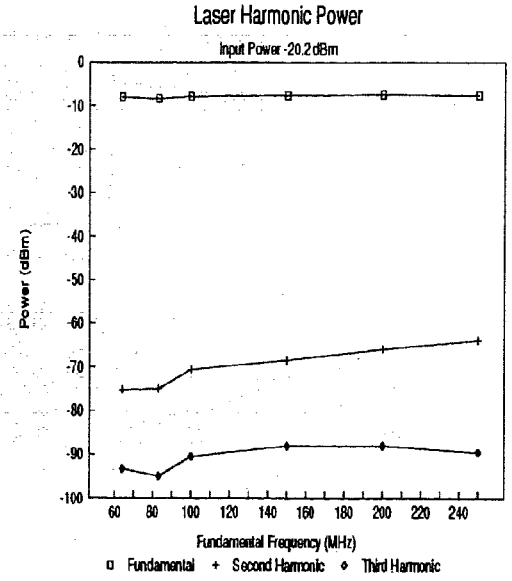

Figure 5.2.5: Measured Harmonic Power for Input of -20.2 dBm

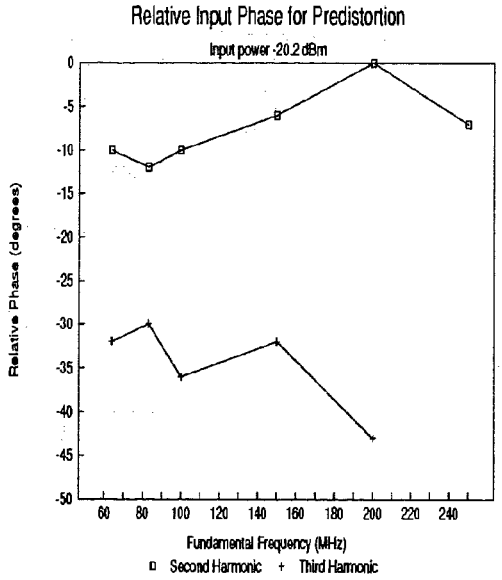

Figure 5.2.6: Measured Harmonic Phase for Input Power of -20.2 dBm

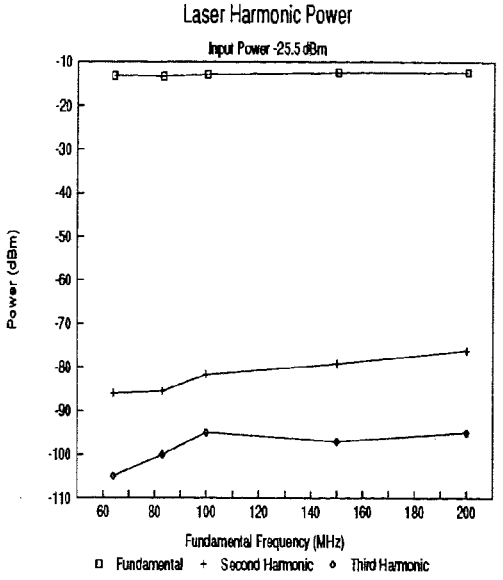

Figure 5.2.7: Measured Harmonic Power for Input of -25.5 dBm

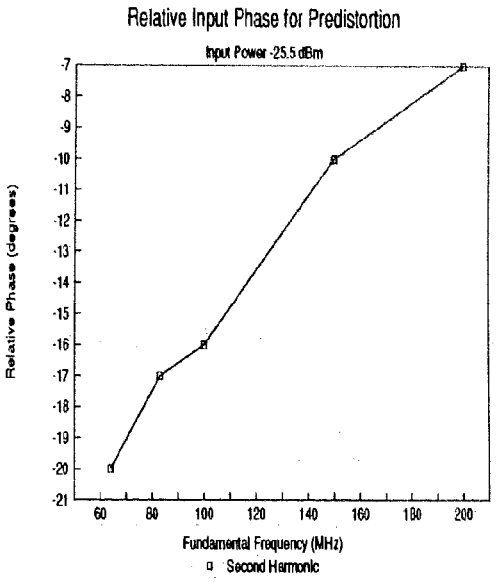

Figure 5.2.8: Measured Harmonic Phase for Input Power of -25.5 dBm

The results show that the second and third order laser polynomial coefficients are frequency dependent. As the input frequency is increased, the harmonic levels increase. Also, the phase of the input harmonics required to cancel the laser's output harmonics do not agree with the real coefficient polynomial model. If the polynomial coefficients for the second and third order coefficients were real, then the phase of the second and third harmonics should have been either +45° or -45° relative to the fundamental for the second harmonic and 0° or -60° relative to the fundamental for the third harmonic. Since neither of these phase values were measured, the polynomial coefficients are complex as well as frequency dependent.

Also, the third harmonic phase and amplitude were difficult to measure due to the very low signal level of the third harmonic. Therefore, the third harmonic phase could only be measured at a high modulation index as shown in the measurement results above.

Some other experiments were performed to determine whether the measured results were caused by the laser. These experiments produced the same values

shown in Figures 5.2.5 to 5.2.8. Therefore, it was determined that the unexpected amplitude and phase characteristics must be due to an unknown internal characteristic of the laser.

However, regardless of the internal characteristics of the laser, the results show what characteristics the optimum predistorter must have in order to predistort the laser. Figure 5.2.9 shows the average measured second and third harmonic phases relative to the fundamental required for the optimum predistorter, and Figure 5.2.10 shows the measured harmonic output power required for the optimum predistorter. The output power required for predistorter was based on the predistorter providing a fundamental input power of -20 dBm into the laser.

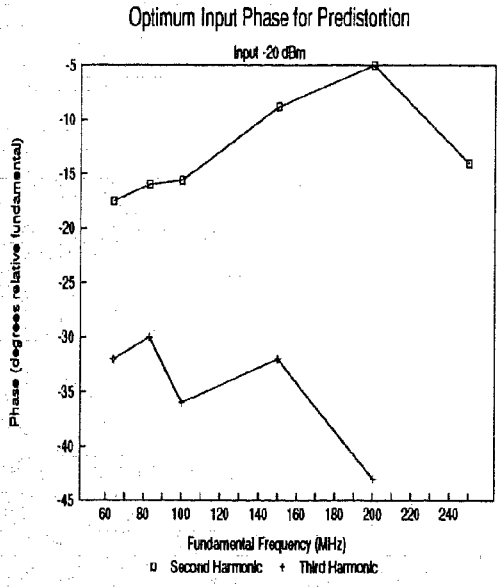

Figure 5.2.9: Measured Optimum Predistorter Phase Characteristic

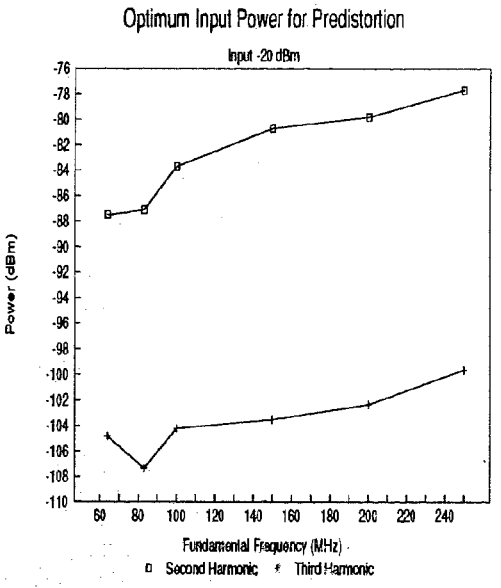

Figure 5.2.10: Measured Optimum Predistorter Amplitude Characteristic

The magnitude and phase of the signals required to predistort the laser do not match the real-coefficient polynomial model. Nonetheless, a predistorter based on the real-coefficient polynomial model was analyzed and constructed in an attempt to verify that a predistorter based on this model could be built and to test its operation. Then, an investigation to determine whether the real-coefficient polynomial predistorter could be altered to account for the characteristics of the laser so that the laser could be predistorted was performed.

5.3 Harmonic Generator Simulation and Fabrication

As mentioned in Section 3, the predistorter must be able to generate second and third order distortion independently. The analysis in Section 4 indicated that independent second and third order distortion could be generated using discrete Schottky diodes. In this section, the second and third order distortion circuits were constructed and tested.

The diodes used to create the harmonic generators to produce the second and third order distortion were Metellics MSS-40 GaAs Schottky diodes. These diodes were selected because they had a very high cutoff frequency (250 GHz) which indicated that the internal parasitic capacitances were very small. Therefore, frequency dependent phase shifts in the 50 - 500 MHz band should have been minimal.

In order to verify that the constructed harmonic generators were operating correctly, a model for the MSS-40 diode that could be used in a simulator was derived.

5.3.1 Diode Model

In order to perform simulations of the harmonic generator circuits, a model for the MSS-40 was required. The I-V characteristic of a sample diode was measured using the HP 7415 Semiconductor Parameter Analyzer, and then an exponential fit to the measured curve was performed using the diode model in PSPICE [21]. The resulting model had the parameters I_s = 1.0 nA, N = 1.214, RS=6, CJO = 0.06 pF, VJ = 0.5 and BV = 3V.

Figure 5.3.1 shows the measured I-V curve vs the modelled I-V curve. The fit to the measured curve is very good. Figure 5.3.2 shows the percent error between the two curves. The error is large for very low voltages because the currents are extremely small. In the typical operating range which will be above 0.3V, the model approximation is acceptable. The error is less than 30% for input voltages above 0.35 V. Thus, the error from using the model should be small.

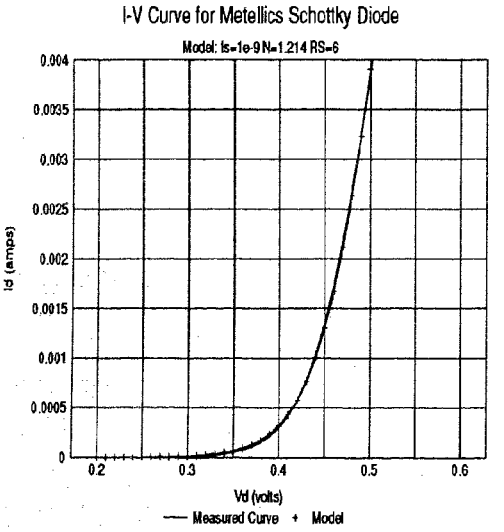

Figure 5.3.1: Measured and Modelled I-V Curves for Metellics MSS-40 Schottky Diode

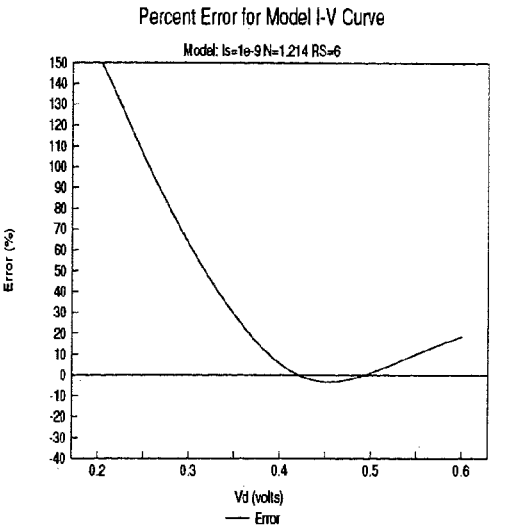

Figure 5.3.2: Percent Error between Measured and Modelled I-V Curves

To determine the levels of the harmonics generated by the diode, a simulation was run using Libra [22]. A schematic diagram of the circuit used in the simulation is shown in Figure 5.3.3. The bias voltage was set to 0.55 V and the input RF power was -10 dBm. Figures 5.3.4 and 5.3.5 show the simulated output power and phase for a number of input frequencies.

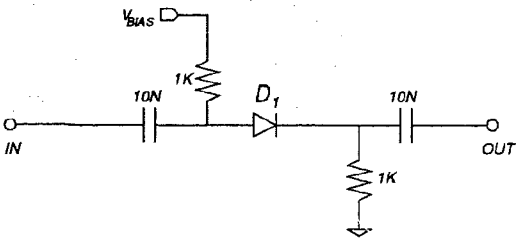

Figure 5.3.3: Diode Harmonic Schematic

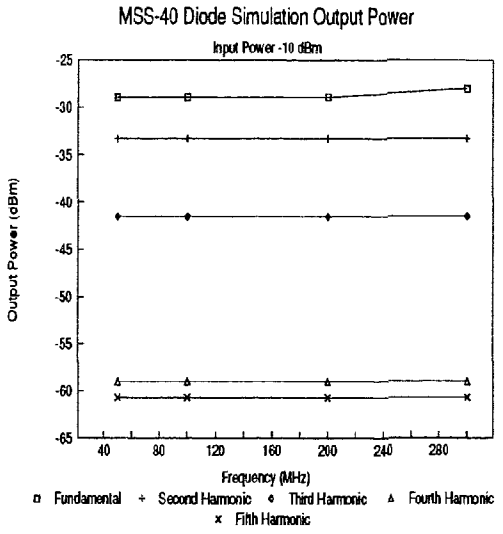

Figure 5.3.4: Simulated Output Power of MSS-40 Diode

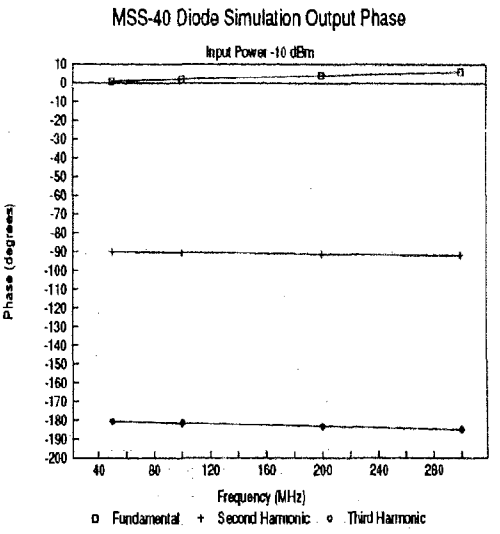

Figure 5.3.5: Simulated Output Phase of MSS-40 Diode

The simulation results indicate that the fourth harmonic is 25.68 dB lower than the second harmonic and the fifth harmonic is 19.16 dB lower than the third harmonic. It is apparent that the first, second, and third harmonics dominate in the system which means that the assumption of a third order model characterizing the diode is reasonably accurate.

The phases of the harmonics agree with the theory presented in Section 4.2, and the results indicate that the diode has positive real coefficients. The simulation also shows that there is a small frequency dependent phase shift. However, the phase changes are all less than 5° which means that cancellation of over 20 dB is still possible across the entire frequency band.

The harmonic levels and their corresponding phases were then measured using an actual MSS-40 diode. The measurement was made with I_{DC} = 90 uA, and V_{BIAS} = 0.529V. The input power was -10 dBm and the measured results are shown in Figures 5.3.6 and 5.3.7.

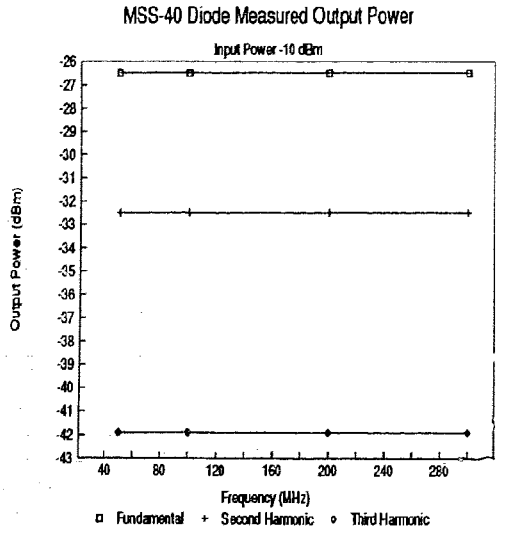

Figure 5.3.6: Measured Output Power of MSS-40 Diode

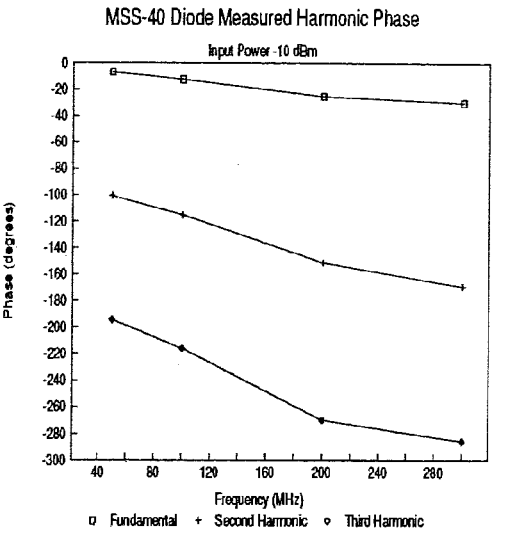

Figure 5.3.7: Measured Output Phase of MSS-40 Diode

The measured amplitudes of the harmonics were within 2 dB of the simulation results which indicated that the diode was performing as expected. However, the phase measurements show that there are frequency dependent phase shifts in all the signals.

Closer examination of the phase measurements indicates that both the second and third harmonic phases are tracking the fundamental phase in accordance with theory. The second harmonic phase is changing at approximately twice the rate of the fundamental phase, and the third harmonic phase is changing at approximately three times the rate of the fundamental phase. Since the second and third harmonic signals have the correct phase with respect to the fundamental signal, the diode can still be used for predistortion.

The phase data in Figure 5.3.7 was obtained using the relative phase measurement technique and then translating the relative phases to the actual phases shown in Figure 5.3.7. The results of the relative phase measurements are simpler to interpret than the actual phase characteristics shown in Figure 5.3.7. Figure 5.3.8 shows the relative phase measurements for the MSS-40 diode.

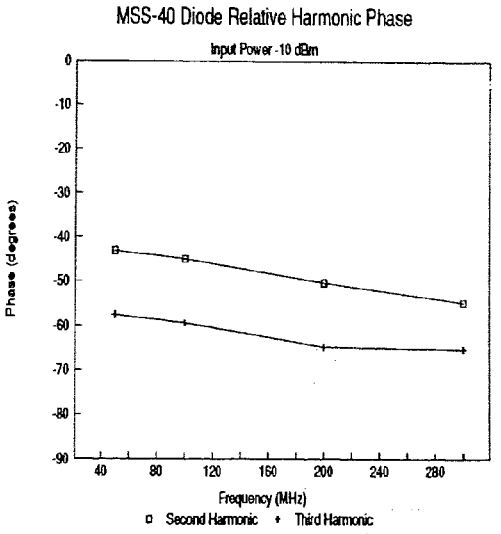

Figure 5.3.8: Measured Relative Phase of MSS-40 Diode

The difference between the measured phase shift of the fundamental and the measured phase shift of the second harmonic was close to -45°. In the same manner, the relative phase shift of the third harmonic was close to -60°. These phase shifts match the phase shifts expected from the theoretical calculations when the polynomial coefficients are positive.

5.3.2 Second Harmonic Generator

The second harmonic generator was constructed using two Schottky diodes in the configuration as shown in Figure 4.1.1. The actual second harmonic schematic diagram is shown in Figure 5.3.9.

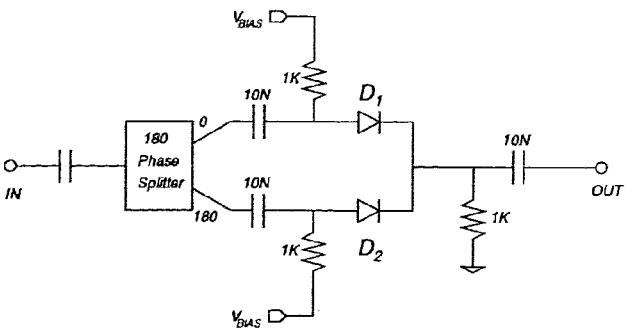

Figure 5.3.9: Second Harmonic Generator Schematic

The bias voltages were set to 0.55V and then adjusted slightly to more effectively cancel the odd order harmonics. With the input power set to -10 dBm and the bias voltage set to 0.559V, the power of the output harmonics were measured for the complete circuit and for the circuit with either diode D1 or D2 biased alone. Table 5.3.1 shows the results. The output power values were constant to within ± 2 dB across the frequency band.

Table 5.3.1: Second Harmonic Generator Output Power

Harmonic	Diode D1 (dBm)	Diode D2 (dBm)	Complete (dBm)
fundamental	-33.1	-33.5	-66.5
second	-41.1	-42.3	-38
third	-52.8	-53.8	-67.5
fourth	-67.5	-67.5	-61.5

The measured output phases of the second harmonic generator relative to the input fundamental at various frequencies are shown in Figure 5.3.10. The output phase for diodes D1 and D2 biased alone and the output phase of the complete second harmonic circuit are shown. In the Figure, D1 Fundamental and D1 Second represent the output fundamental and output second harmonic phases relative to the input fundamental of diode D1 when diode D1 is biased alone. Similarly, D2 Fundamental and D2 second represent the output phases when diode D2 is biased

alone. Combined second refers to the output second harmonic relative to the input fundamental when both of the diodes are biased together to form the second harmonic generator.

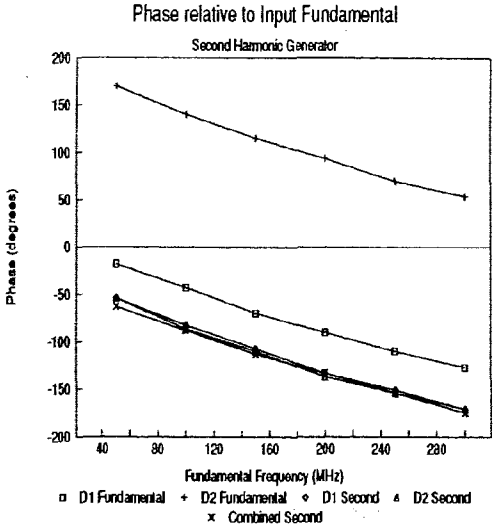

Figure 5.3.10: Measured Relative Phase of Second Harmonic Generator

From Figure 5.3.10 it is clear that the phases of the fundamentals from each of the diodes are 180° out of phase with each other and their powers cancel. The phases of the second harmonic from each diode are almost the same and are approximately equal to the output phase of the second harmonic from the complete circuit. This result is expected since the second harmonics should add in phase. The output phase of the fundamental from the complete circuit is not meaningful since its value depends heavily on the amount of cancellation and the amplitude and phase imbalance. The output second harmonic has the correct phase relationship with the uncanceled output fundamental in that the second harmonic lags the fundamental by 45°. This 45° phase shift is seen as the constant difference between the fundamental and second harmonic curves in Figure 5.3.10. Thus, the second harmonic generator circuit produces a frequency independent second harmonic.

The small variations from the theoretical values in the measured phases are likely due to any one or more of the following problems. The 180° phase splitter has a phase imbalance between the two output ports of up to 5° and an amplitude

imbalance of up to 0.3 dB. Therefore the two arms of the circuit may have slightly different output powers and phases. Also, the phase measuring procedure outlined in Section 5.1 has uncertainty associated with it as already described.

5.3.2.1 Simulation Results

The second harmonic generator was also simulated using Libra. Table 5.3.2 shows the output power from the simulation with one diode biased and with both diodes biased. The bias voltage was set to 0.55V and the input power was set to -14 dBm to account for the loss of the power splitter in the physical circuit. The simulator used ideal power splitters with no loss.

Table 5.3.2: Simulated Second Harmonic Generator Power

Harmonic	Diode D1 (dBm)	Diode D2 (dBm)	Complete (dBm)
fundamental	-31.4	-31.4	-318.7
second	-38.0	-38.0	-34.0
third	-50.3	-50.3	-328.9
fourth	-84.3	-84.3	-65

The simulated power levels for the complete second harmonic generator were close but slightly larger than the measured results. However, the simulated results were within 2 dB of the measured values when only one diode was biased. The difference in the complete circuit simulation was likely due to the ideal cancellation situation occurring in the simulation. The odd order powers in the simulation cancel almost perfectly, whereas in reality, perfect cancellation is difficult to achieve. The power that was measured in the odd order harmonics in the measured circuit will be directed into the even order harmonics in the simulation and will make the simulation numbers larger.

The phase of the second harmonic generator simulation is shown in Figure 5.3.11.

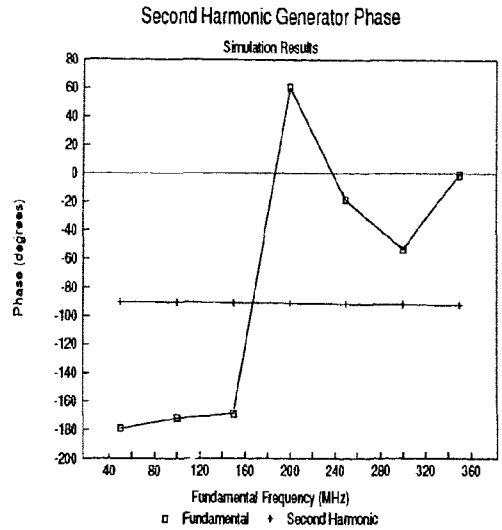

Figure 5.3.11: Simulated Phase of Second Harmonic Generator

In Figure 5.3.11 it is clear that the phase of the second harmonic is constant but the phase of the fundamental is highly variable. This result was expected from Section 4.2, and shows why the output fundamental from the second harmonic generator can not be used as a reference for measuring the output phase of the second harmonic generator.

5.3.3 Third Harmonic Generator

The third harmonic generator was constructed using two anti-parallel diodes as shown in Figure 4.1.2. The complete schematic diagram of the third harmonic generator is shown in Figure 5.3.12.

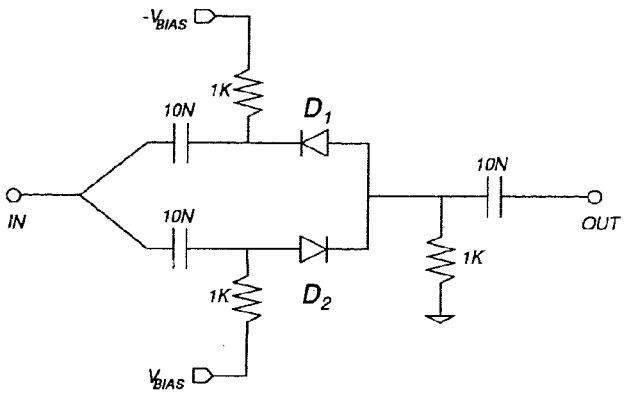

Figure 5.3.12: Third Harmonic Generator Schematic

The third harmonic generator was tested with the bias voltages optimized to +0.683V for diode D2 and -0.672V for diode D1. The input power was set to -10 dBm, and the output power was measured with diodes D1 and D2 biased alone and with them both biased together. The results for frequencies between 50 MHz and 300 MHz are shown in Table 5.3.3. The values were within ± 2 dB across the frequency band.

Table 5.3.3: Third Harmonic Generator Output Power

Harmonic	Forward D2 (dBm)	Reverse D1 (dBm)	Complete (dBm)
fundamental	-27.6	-28.0	-19.8
second	-36.2	-36.2	-70
third	-45.5	-45.3	-42.9
fourth	-64.5	-64.0	< -80

The measured output phases relative to the input fundamental for the complete third harmonic circuit are shown in Figure 5.3.13.

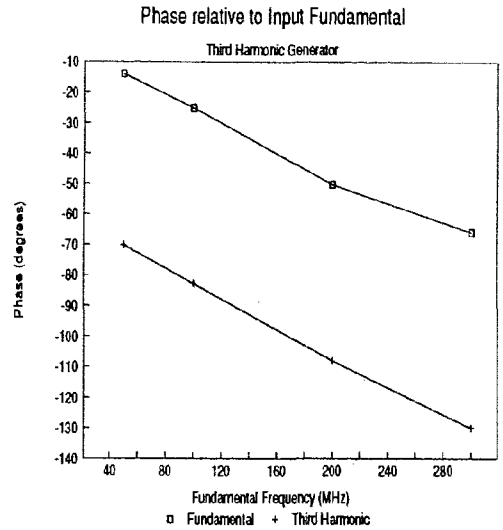

Figure 5.3.13: Measured Relative Phase of Third Harmonic Generator

The measured output phase of the third harmonic generator is very close to -60° as seen in Figure 5.3.13. This indicates that the third harmonic is in phase with the fundamental as expected. Thus the circuit produces a frequency independent fundamental and third harmonic from 50 MHz to 300 MHz.

5.3.3.1 Simulation Results

The third harmonic generator was also simulated using Libra. The bias voltages were set to ± 0.65 V and the input power was -10 dBm. Table 5.3.4 shows the output power from the circuit when only one of the diodes was biased and when both of the diodes were biased.

Table 5.3.4: Simulated Third Harmonic Generator Power

Harmonic	Forward D2 (dBm)	Reverse D1 (dBm)	Complete (dBm)
fundamental	-26.97	-26.97	-17.10
second	-32.05	-32.05	< -200
third	-41.94	-41.94	-38.25
fourth	-80.51	-80.51	< -200
fifth	-58.48	-58.48	-53.15

The simulated output powers are close to the measured values. Like the second harmonic generator simulations, the results for the single diode biased alone are closer to the measured values than the results with both diodes biased. The simulation output powers for the complete third harmonic generator are 2 and 4 dB higher than the measured results, but the even order harmonics in the simulation are negligible whereas in the real circuit there is still measurable power in these harmonics which will reduce the power available to the odd order harmonics.

Figure 5.3.14 shows the output phases of the fundamental and third harmonics from the simulation. The simulation incorporated a -10° phase shift in the input fundamental signal.

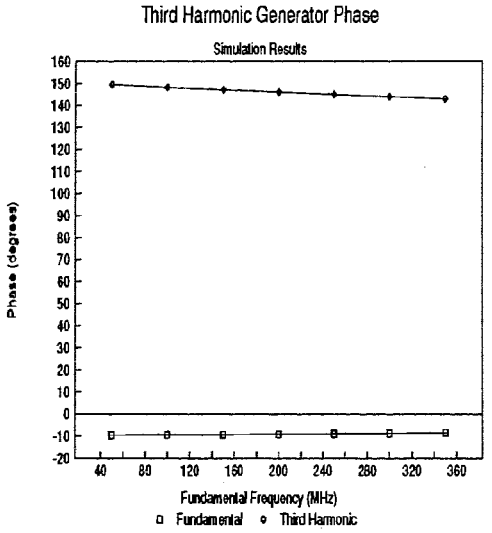

Figure 5.3.14: Simulated Phase of Third Harmonic Generator

The fundamental and third harmonic phases agree with the values predicted in Section 4.2. The second harmonic phase was variable and depended on the amount of cancellation as indicated in equations (4.2.17) and (4.2.18).

The simulations and experimental results indicate that both the second and the third harmonic generators are operating as expected. Also, the measured results indicate that the unwanted third harmonic produced by the second harmonic generator was 30 dB down, as was the unwanted second harmonic

produced by the third harmonic generator. Therefore, as long as the second and third harmonics required by the predistorter are within about 10-15 dB of one-another, then the unwanted harmonics will contribute a negligible effect.

5.4 Predistorter Construction

The predistorter was constructed using the second and third harmonic generators described in the previous section. A block diagram of the predistorter is shown in Figure 5.4.1.

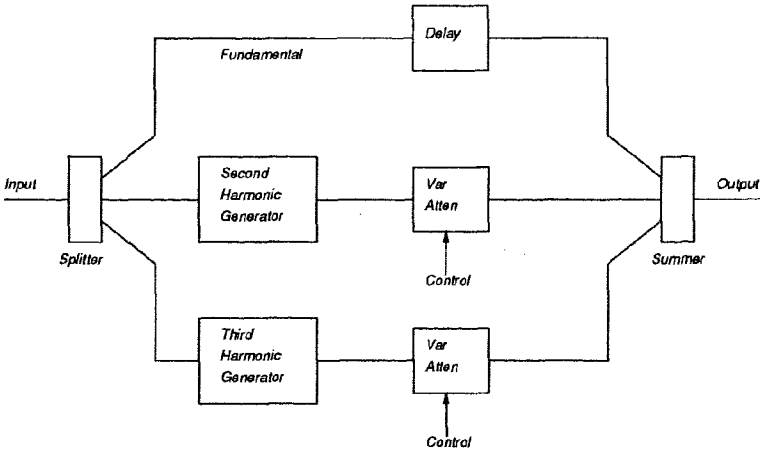

Figure 5.4.1: Block Diagram of Predistorter

The input signal was split three ways to provide the required input signals for the fundamental path, the second harmonic generator, and the third harmonic generator. A delay line was incorporated into the fundamental path to account for the signal delays that occurred through the harmonic generators and attenuators so that the output fundamental and harmonic signals had the correct phase relationship when they were summed to form the output signal.

The coefficients of the second and third harmonics were adjusted using the variable attenuators. The control signals to the variable attenuators were for fine tuning the coefficients and would be used to control the coefficients in an adaptive loop.

Based on the laser model and the way that the laser was biased, the laser diode was a "reverse" biased diode as described in Section 4.2. Therefore, the laser input/output function was expected to be

$$I_{laser} = aV - bV^2 + cV^3 - \ldots \quad (5.4.1)$$

Thus, the predistorter polynomial was expected to be

$$I_{predist} = aV + bV^2 - cV^3 - \ldots \quad (5.4.2)$$

To ensure that the predistorter's second order coefficient was positive and its third order coefficient was negative, the phase of the second harmonic was required to be -45° relative to the fundamental, and the phase of the third harmonic was required to be 0° relative to the fundamental.

5.4.1 Building the Predistorter

The predistorter was constructed to provide the input/output relationship of (5.4.2). Thus, the second harmonic required a -45° phase shift relative to the fundamental and the third harmonic required a 0° phase shift relative to the fundamental. These signal dependencies were accomplished by using 0° and 180° power splitters. The input signal was passed into a 0° power splitter and the two outputs were then passed into 180° power splitters. One of the 180° power splitters provided the ±V signals for the second harmonic generator, and the other 180° power splitter provided the input for the third harmonic generator and the input for the fundamental delay path. The 180° output was connected to the third harmonic generator input so that the third harmonic output would have a 0° phase shift relative to the fundamental. Figure 5.4.2 in the next section shows the arrangement of these splitters. The splitter configuration ensured that the signal delays through each path were approximately the same since all the paths were routed through similar elements. A detailed schematic diagram of the predistorter is contained in Appendix A.

The Metellics MSS-40 diodes were used for the harmonic generators and the harmonic generator circuits described in Section 5 were used without modification. The variable attenuators were realized using MA/COM Model AT-250 voltage

variable absorptive attenuators that had a frequency range from DC - 2 GHz and a 13 dB variable attenuation range. A 3-way 0° power summer was used to combine the fundamental, second, and third harmonics at the output of the predistorter.

Individual power supplies for the bias lines were also incorporated into the design so that the bias current of the diodes could be tuned to obtain the largest amount of cancellation in the harmonic generators. This was to account for mismatches between the individual diodes.

5.4.1.1 Design Issues During Construction

During fabrication and testing of the predistorter, a number of difficulties were encountered.

The first difficulty was caused by amplitude and phase imbalance between the ports of the power splitters and power summers. The output ports of a power splitter had a potential amplitude imbalance of up to .5 dB and a phase imbalance of up to 6°. Thus, the amplitude and phase of the input signals to the harmonic generators from each splitter port were not identical, and caused mismatches in the harmonic generator output amplitude and phase.

The second harmonic generator required the signals from both sides of the splitter. The amplitude and phase imbalance between the two ports resulted in less cancellation of the odd order harmonics since the harmonic phase and power levels were slightly mismatched. However, the actual second harmonic signal was not affected as much since the signals were adding in phase. With the imbalances, the odd order harmonics were still more than 30 dB below the second harmonic.

The third harmonic generator was affected by phase imbalance. Any phase imbalance in the output of the splitter to the third harmonic generator resulted in the third harmonic shifting by three times this value. This effect also occurred in the second harmonic path, the phase shifts being two times the error. These extra phase shifts meant that the output signals of each harmonic path could be

up to 6° out of phase with each other, thus reducing the amount of cancellation possible. To correct for these errors, appropriate lengths of transmission line had to be added to each path to re-align the phases.

Another difficulty was due to back reflection and isolation effects from the harmonic generators and the power splitters. Figure 5.4.2 shows a block diagram of the predistorter with labels at various points. Signals will be described as passing from one point to another.

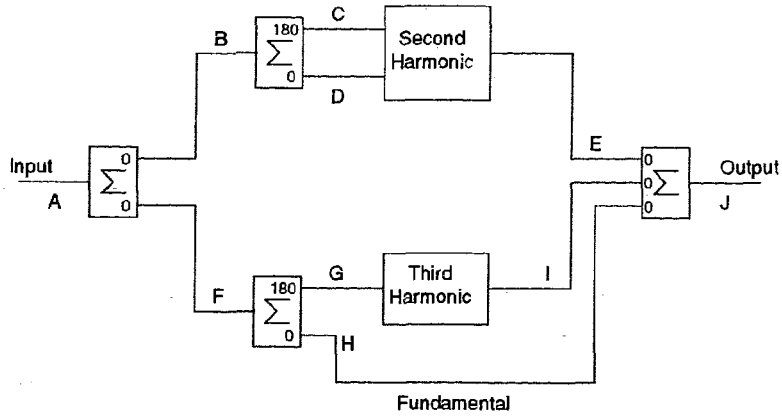

Figure 5.4.2: Back Reflection and Isolation Diagram

During testing, it was found that some of the third harmonic power from the third harmonic generator at point I was appearing on the fundamental output line of the predistorter at point H when the outputs of the fundamental, H, second, E, and third, I, harmonic generators were not connected to the output power summer. This third harmonic was caused by some of the third harmonic power reflecting off the third harmonic generator due to the mismatch between the diodes and the power splitters. The reflected third harmonic at G then passed through the 2-way power splitter and appeared on H. The isolation between points G and H was approximately 20 dB, so the reflected signal at G was 20 dB higher than the signal at H.

There was also another complication caused by the poor isolation of the power splitters. When all the paths of the predistorter were connected, the fundamental power level at H was considerably higher than the harmonic power

levels at E and I. However, a portion of the signal power at H appeared at I and E due to poor isolation, and passed backwards through the harmonic generators. These backward signals were especially damaging to the third harmonic path when the output third harmonic level was very low. The backward signals through the third harmonic generator generated additional third harmonic signals since the third harmonic generator is bi-directional. This caused the third harmonic at the output J to attain power levels that could not be controlled properly with the third harmonic attenuator because the unwanted signals had the opposite phase to the wanted signals and they combined in a destructive manner. This only occurred when the third harmonic output power was very low. At high output powers, the reflection and isolation problems were insignificant.

The reflections could have been eliminated using appropriate matching techniques to match the diode input to the power splitter output. Unfortunately, wideband matching is very difficult and was not an option. The reflections and isolation complications could have been eliminated by placing isolators at points B, C, D, E, F, G, and H. However, isolators were not available and would have been too expensive. Therefore, the isolation was increased by simply adding fixed attenuators to the power splitter outputs at points B and G. The attenuators helped reduce the back reflections, but they also reduced the output power of the harmonic levels. Attenuators were also added at points E and I to reduce the harmonic levels to the appropriate level for predistortion.

A 3 dB attenuator was placed before the third harmonic generator and a 5 dB attenuator was placed before the second harmonic generator. Also, a 50 ohm resistor was placed in shunt across the input power splitter which helped attenuate the reflected signals.

When the final output levels were attained, the second and third harmonic signals had the correct amplitude and phase response and were minimally effected by the reflection and isolation concerns.

Aligning the output phases of the fundamental, second, and third harmonics was also difficult. The fundamental signal required a phase shift to account for the delay through the diodes in the harmonic generators. This phase shift was realized using a length of transmission line. Unfortunately, the phase measurements required to calculate the length of the transmission line were not very accurate, so it was optimized using trial and error.

The variable attenuators used to adjust the coefficients had a small frequency dependent phase shift. The amount of the phase shift was dependent on the control voltage (attenuation level) and the frequency. For frequencies below 200 MHz, the phase shift was within ± 5 °, and at 500 MHz the phase shift varied between +3° and -12°. Therefore, the third harmonic output phase for higher input frequencies may be shifted by up to 12°. This corresponds to cancellation of approximately 13 dB if the amplitude is correct. Figure 5.4.3 shows the measured amplitude response of the attenuator for various control voltages.

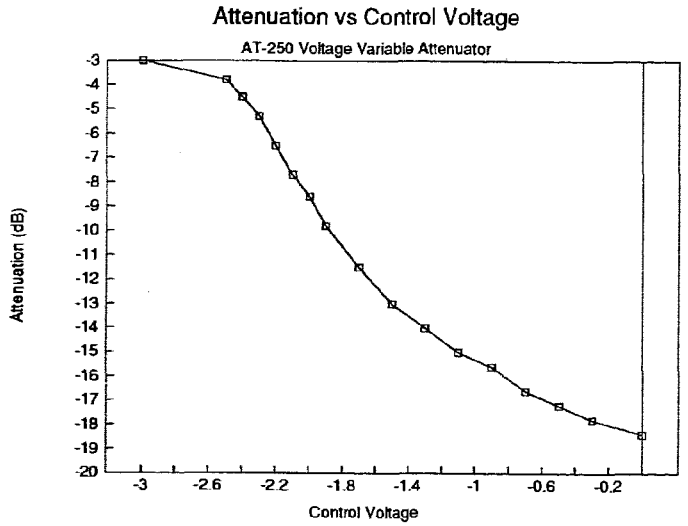

Figure 5.4.3: Measured Attenuation vs Control Voltage for AT-250 Attenuator

The attenuator had an attenuation range of approximately 15 dB. The centre of the attenuation range occurred at a control voltage of approximately

-1.8V. The predistorter output power level was set so that the expected distortion level occurred at -1.8V. Hence, up to ± 7 dB of fine tuning was available to attain full cancellation when predistorting a non-linear device.

There was no way of easily accounting for the phase response of the attenuator. The predistorter output phases were aligned with the control voltage set at -1.8 V. The phase changes that occurred when the attenuation was varied resulted in phase imbalances at the output. However, since these phase changes were relatively small as mentioned, the predistorter should still be able to operate across the frequency band with good results.

5.4.1.2 Measured Predistorter Outputs

The predistorter output characteristics are summarized in Table 5.4.1 for an input power of -10.0 dBm. In the second harmonic path, there was a fixed 5 dB attenuator before the input to the second harmonic generator and a fixed 10 dB attenuator at the output of the second harmonic generator before the variable attenuator. The third harmonic path had a fixed 3 dB attenuator before the third harmonic generator and a fixed 3 dB attenuator at the output before the variable attenuator. These attenuators were used to reduce the second and third harmonic signals to the desired power level and to minimize the back reflection effects.

Table 5.4.1: Measured Predistorter Output

Signal	Power (dBm)	Relative Phase
Fundamental	-26.5	0°
Second	-81 to -66	-45°
Third	-97 to -83	0°

The second and third harmonic power level ranges can be changed by varying the values of the fixed attenuators to achieve the range required to predistort a given non-linear device.

5.5 Predistortion of a Schottky Diode

A preliminary test to determine whether the predistorter worked was performed by using the predistorter to linearize an MSS-40 Schottky diode. The schottky diode was "reverse" biased, and the bias level was chosen so that the diode's output harmonics were in the range of the predistorter harmonics.

The fundamental output power from the predistorter was -26.5 dBm when the input power was -10 dBm. If -26.5 dBm was supplied to the MSS-40 diode, the output fundamental was -29.5 dBm, the output second harmonic was -71.7 dBm, and the output third harmonic was -99 dBm when the bias voltage for the diode was -3.6V.

The predistorter was then inserted before the MSS-40 diode and the variable attenuators were varied to obtain the largest amount of cancellation of the harmonics. The predistorter was able to reduce the level of the second harmonic by 15 dB to 3 dB across the 50 MHz to 330 MHz band. However, the third harmonic did not predistort at all. It appeared that the third harmonic distortion of the predistorter was adding in phase with the third harmonic distortion of the diode instead of cancelling it. Therefore the MSS-40 diode was tested to determine the effect of the phase of the harmonics when the bias current was varied.

Figure 5.5.1 shows the output power of each of the harmonics for a "reverse" biased MSS-40 diode at various bias voltages and Figure 5.5.2 shows the phase of the harmonics at the same bias voltages. The input power to the diode was -10.5 dBm at a frequency of 70 MHz. The phase plot shows the phase of the second and third harmonics with respect to the fundamental in degrees relative to the fundamental.

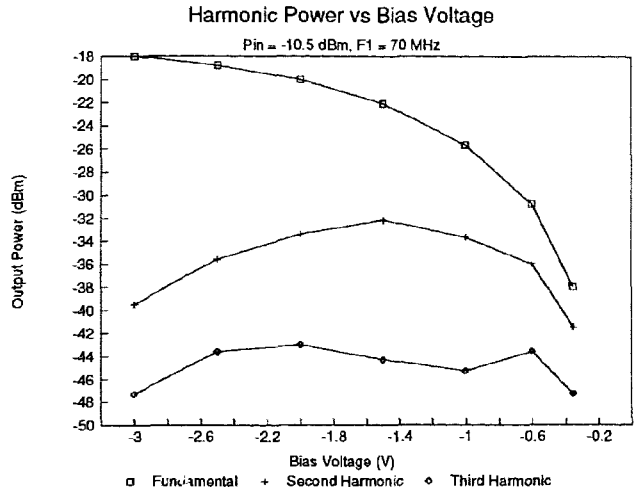

Figure 5.5.1: Measured Harmonic Power vs Bias Voltage for "reverse" biased MSS-40 Diode

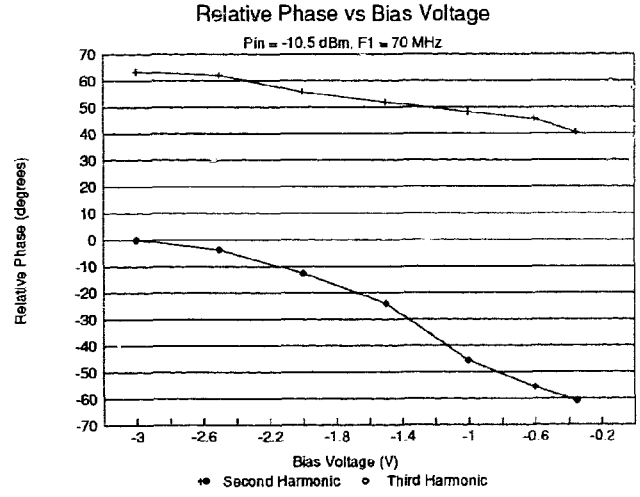

Figure 5.5.2: Measured Harmonic Phase vs Bias Voltage for "reverse" biased MSS-40 Diode

From Figure 5.5.2, the phase of the third harmonic changed from -60° to 0° as the bias voltage was decreased from -0.3V to -3.6V. The 60° change in the relative third harmonic phase corresponded to an actual change in phase of 180° in the third harmonic. The second harmonic stayed relatively constant at -45° with respect to the

fundamental which explained why it could be predistorted. Since the bias voltage used for the diode was -3.6V, the predistorter's third harmonic was in phase with the diode third harmonic so predistortion of the third harmonic did not occur.

A Libra simulation was performed to determine whether the bias dependent phase shift of the third harmonic was expected. The simulation showed that the 180° phase change in the third harmonic did occur which verified the measured results.

The 180° phase splitter on the predistorter used for the third harmonic generator was replaced with a 0° phase splitter to get the third harmonic in the correct phase with the fundamental. When this change was implemented, the third harmonic could be reduced by 10 dB for fundamental signals between 60 MHz and 80 MHz.

Figure 5.5.3 shows the fundamental signal levels in the circuit for input frequencies between 60 MHz and 80 MHz. The input power level was -7 dBm, the predistorter output level was -23 dBm, and the system output level was -26 dBm. The test frequencies of 60 -80 MHz were used since a bandpass filter in this frequency band was available. The input signal generator harmonics were larger than the harmonics generated by the predistorter and the diode so the signal generators harmonics had to be reduced through filtering.

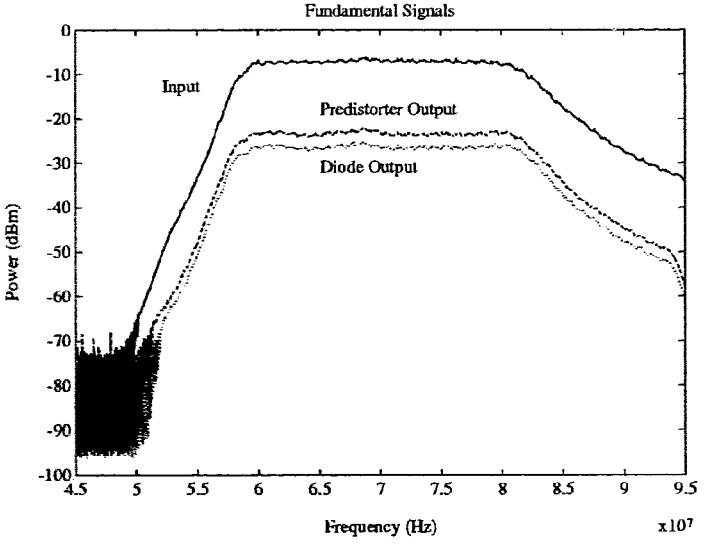

Figure 5.5.3: Measured Fundamental Signals

Figure 5.5.4 shows the second harmonic output for the input signal in Figure 5.5.3. The predistorter output second harmonic was -65 dBm and the second harmonic from the diode with the predistorter turned off was -68 dBm. With the predistorter turned on, the second harmonic varied from -90 dBm to -78 dBm which was an improvement of 22 dB to 10 dB.

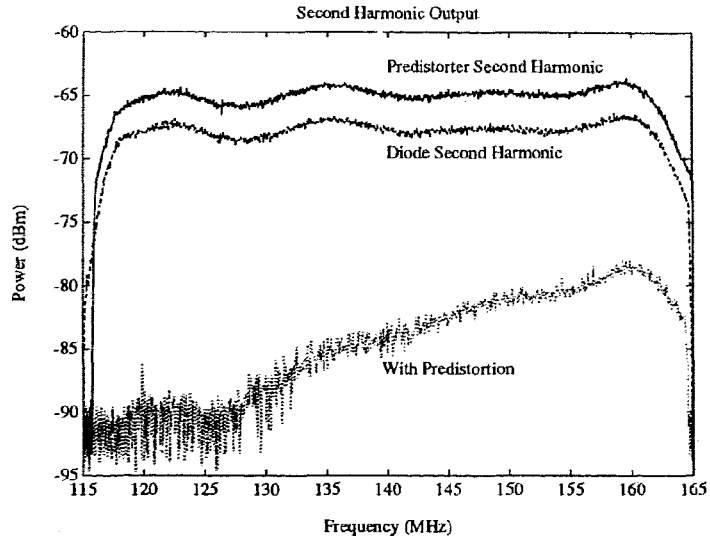

Figure 5.5.4: Measured Second Harmonic Signals

Figure 5.5.5 shows the third harmonic output signals for the input signal in Figure 5.5.3. The predistorted output shows an improvement of 19 dB to 8 dB.

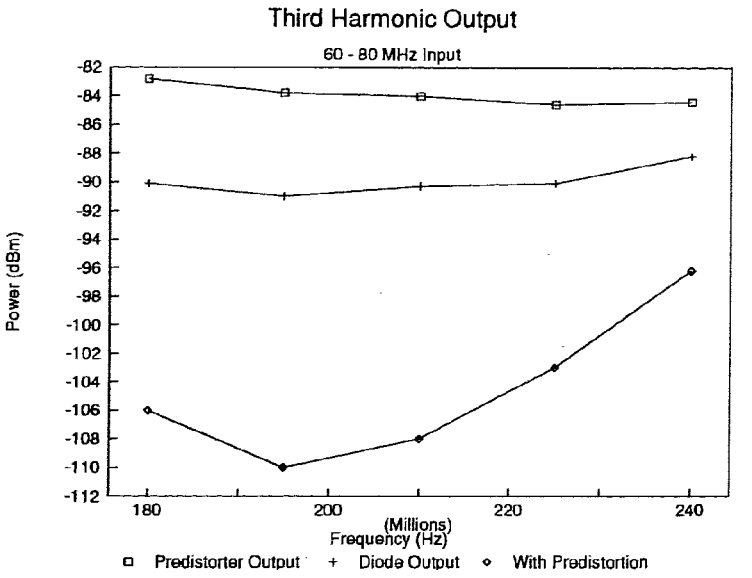

Figure 5.5.5: Measured Third Harmonic Signals

Figure 5.5.5 shows that the cancellation of the third harmonic degraded as the frequency was increased. This was due to the amplitude imbalance of the predistorter and diode signals. The predistorter third harmonic amplitude was getting smaller as the frequency was increased whereas the third harmonic from the diode was getting larger as the frequency was increased. If the predistorter attenuator was adjusted at the higher frequencies, then the high frequencies showed large cancellation and the low frequencies showed less cancellation. This indicated that the phase of the predistorter signal was correct at all frequencies and the amplitude changes were affecting the amount of third harmonic cancellation.

5.5.1 Verification of Polynomial Equation for Predistortion

To test whether the predistorter was operating according to the polynomial model, the actual polynomial coefficients were derived for the diode, the predistorter, and the composite system for the schottky diode test and compared with the results of equations (3.1.1) to (3.1.4).

Equation (5.5.1) summarizes the polynomial input/output equation.

$$V_o = aV - bV^2 + cV|V|^2, \tag{5.5.1}$$

If a sinusoidal voltage, V, is applied to the input, then the output fundamental and harmonic voltages are

$$V_{fund} = \left(aV + \frac{3}{4}cV^3\right)\sin(\omega t + \theta), \tag{5.5.2}$$

$$V_{second} = b\frac{V^2}{2}\sin(2\omega t + 2\theta + 90°), \tag{5.5.3}$$

$$V_{third} = c\frac{V^3}{4}\sin(3\omega t + 3\theta + 180°), \tag{5.5.4}$$

The power in these voltages is equal to the voltage squared divided by the resistance the power is measured through. Thus, equations (5.5.2) to (5.5.4) can be re-arranged to find the magnitude of the coefficients of (5.5.1) from the power measurements. The equations for calculating the magnitude of the coefficients are shown below. The signal V_{RMS} is the input voltage.

$$V_{RMS} = \sqrt{R \cdot \log^{-1}\left(\frac{P_{in} - 30}{10}\right)}, \tag{5.5.5}$$

$$b = \frac{2}{V_{RMS}^2}\sqrt{R \cdot \log^{-1}\left(\frac{P_2 - 30}{10}\right)}, \tag{5.5.6}$$

$$c = \frac{4}{V_{RMS}^3}\sqrt{R \cdot \log^{-1}\left(\frac{P_3 - 30}{10}\right)}, \tag{5.5.7}$$

$$a = \frac{1}{V_{RMS}}\sqrt{R \cdot \log^{-1}\left(\frac{P_1 - 30}{10}\right)} - \frac{3cV_{RMS}^3}{4}, \tag{5.5.8}$$

where P_{in}, P_1, P_2, and P_3 are the average powers of the input, output fundamental, output second harmonic, and output third harmonic respectively, measured in dBm, and R is the load resistance the power is measured across (50 ohms).

The sign of the coefficients is determined from the measured phase. Also, the fundamental coefficient cannot be determined correctly until the sign of the third order coefficient is determined. However, the third order coefficient is generally too small to make any significant effect so the third order term can generally be ignored in (5.5.8).

Using the equations given in (5.5.5) to (5.5.8), the coefficients for equation (5.5.1) can be derived. The coefficients, a, b, and c, can then be substituted for $\alpha_1, \alpha_2, \alpha_3, \beta_1, \beta_2, \beta_3$, or $\zeta_1, \zeta_2, \zeta_3$ to obtain equations (3.1.1) to (3.1.3) depending on which signals are being measured. For example, when the MSS-40 schottky diode was used as the non-linear device, an input power of -23 dBm to the MSS-40 diode produced a fundamental output at -26 dBm, a second harmonic at -68 dBm, and a third harmonic at -89 dBm. This results in a, b, and c, corresponding to β_1, β_2, and β_3 respectively, and the polynomial expression for (3.1.2) becomes

$$V_d = 0.7064V_p - 0.7105V_p^2 - 8.000V_p^3. \tag{5.5.9}$$

The coefficients for the second and third harmonics are negative since the phase of the harmonics were +45° and 0° with respect to the fundamental.

In the same manner, the polynomial expression for the predistorter, equation (3.1.1), can be obtained. The input to the predistorter was -7 dBm, and the output fundamental, second harmonic, and third harmonic were -23 dBm, -65 dBm, and -84 dBm respectively. These values result in the polynomial expression for (3.1.1) being

$$V_p = 0.1581V_m + 0.0252V_m^2 + 0.0566V_m^3. \tag{5.5.10}$$

Using equation (3.1.4), the polynomials for the composite system (3.1.3) can be calculated. The result is

$$V_a = 0.11165V_m + 0.000057V_m^2 + 0.002838V_m^3. \tag{5.5.11}$$

These polynomials result in the output powers of -26 dBm, -118 dBm, and -110.5 dBm for the fundamental, second, and third harmonics respectively for an input power of -7 dBm. The composite polynomial equation can also be found from the measured results. From the measured results for the composite system, an input power of -7 dBm produced output values of -26 dBm, -90 dBm, and -110 dBm for the fundamental, second harmonic, and third harmonic respectively. These values result in the polynomial equation

$$V_a = 0.1122V_m + 0.0014V_m^2 + 0.0028V_m^3. \tag{5.5.12}$$

This equation has similar first and third order coefficients compared to (5.5.11), but the second order coefficient is larger. If the predistorter polynomial coefficients are derived from (5.5.12) and (5.5.9) using (3.1.4), the result is

$$V_p = 0.15805V_m + 0.0272V_m^2 + 0.0573V_m^3, \quad (5.5.13)$$

which corresponds to output powers of -23 dBm for the fundamental, -64.4 dBm for the second harmonic, and -83.9 dBm for the third harmonic when the input power is -7 dBm. These derived values are within 1 dB of the measured signals used to form equation (5.5.10). Thus, the power levels have a large effect on the derivation of the composite polynomial equation. However, the results also show that the equations match the measured results indicating that the circuit is performing in accordance with the third order polynomial model.

5.6 Predistorter Modification for Operation with Laser

The basic predistorter operation using the third order model was verified using a schottky diode as the non-linear device. From Section 5.2, the laser did not behave in the same manner as the schottky diode. In this section, modifications made to the predistorter to achieve the necessary signal characteristics to predistort the laser are described.

The first modification required for the predistorter was to have it produce second and third order distortion at the appropriate power level needed for the laser. Since the predistortion levels required by the laser were lower than those required by the schottky diode, fixed attenuators were added to the outputs of the second and third harmonic generators.

A 20 dB attenuator was added to the second harmonic generator and a 30 dB attenuator was added to the third harmonic generator. Unfortunately, the corresponding output level of the third harmonic generator became too small to control accurately using the given circuit architecture. The isolation and back reflection effects discussed in Section 5.4.1.1 were significant, and an independently controllable third harmonic with the correct phase response could not be generated. Therefore, the third harmonic generator was disconnected and predistortion with only the second harmonic generator was investigated.

The power levels required for second harmonic predistortion were achievable using the current circuit configuration and the attenuator. However, the phase of the predistorter second harmonic was still -45° with respect to the fundamental. For the laser, the phase of the second harmonic varied from -17° to 0° between 60 and 200 MHz as was shown in Figure 5.2.9. Between 100 and 200 MHz, the phase of the required second harmonic had an approximately linear slope.

The predistorter required an element to delay the fundamental signal so that the relative phase difference between the fundamental and the second harmonic was reduced. The fundamental signal needed to be delayed by approximately 22° at 100 MHz and 45° at 200 MHz. This was accomplished by adding an appropriate length of transmission line to the fundamental path. Transmission line has a linear phase response, so the predistorter also had a linearly changing relative phase response between the fundamental and the second harmonic. Figure 5.6.1 shows the measured phase of the predistorter second harmonic and the optimum phase required by the laser for predistortion after the delay line had been added.

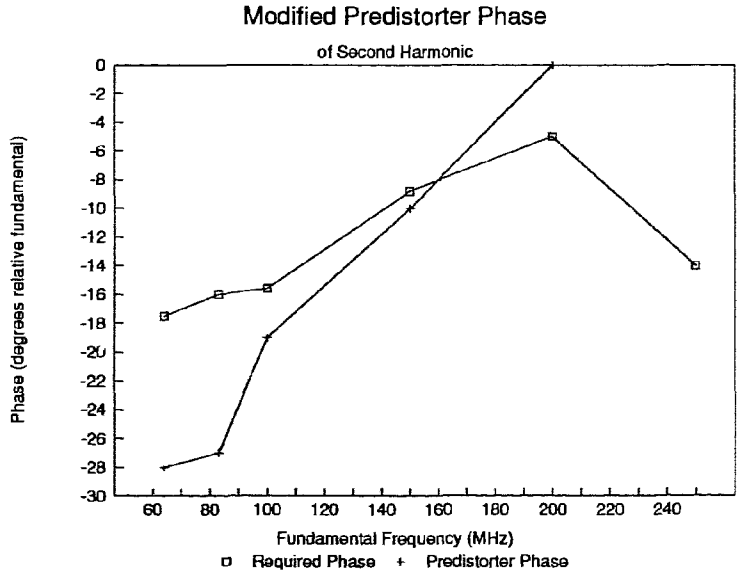

Figure 5.6.1: Measured Predistorter Phase vs Optimum Predistorter Phase

Figure 5.6.1 shows that the phase of the predistorter closely matches the phase required by the laser between 100 MHz and 200 MHz. Below 100 MHz, the phase of the predistorter diverges, and is 10° in error at 64 MHz. This translates to a 20° error for the actual second harmonic signal. Therefore, the maximum attenuation expected at 64 MHz would be 9 dB if the amplitude was correct.

The amplitude of the second harmonic generated by the predistorter must also have the same amplitude response with frequency as shown in Figure 5.2.10 to provide complete cancellation. The predistorter thus needs to produce a frequency dependent output power level which increases with frequency. This could be achieved by building an equalizer on the predistorter. Ideally, the equalizer would have the combined phase and amplitude response necessary to modify the original predistorter to predistort the laser. Thus, a simple equalization block could be added to the second harmonic path in the predistorter which would keep the predistorter architecture general.

The ideal equalizer would be constructed from filter sections which produce the required amplitude and phase response. However, the design of an equalizer is not trivial, so the amplitude response of the predistorter was left unchanged. Therefore, the predistorter should be able to cancel the second harmonic of the laser at individual frequencies across the band by adjusting the variable attenuator at each frequency. If a plot of the attenuator level vs frequency is made, then the attenuator level should track the required input power level needed for the laser. If the attenuator is fixed, a smaller wideband cancellation, likely between about 100 MHz and 200 MHz should be seen.

6 PREDISTORTED LASER

This section contains the measured results of the cascade of the modified predistorter and the laser for both single and multiple input signals.

6.1 Single Tone Predistortion of Second Harmonic

The first test performed with the predistorter was to measure the amount of cancellation obtainable at each frequency with the predistorter attenuator adjusted for optimal cancellation. Figure 6.1.1 shows the fundamental input signal from the predistorter (Input Fund), the fundamental output signal from the laser (Laser Fund), the second harmonic from the laser without predistortion (Laser Second), the second harmonic from the laser with predistortion (With Predistortion), and the level of the predistorter second harmonic output (Predistorter Second).

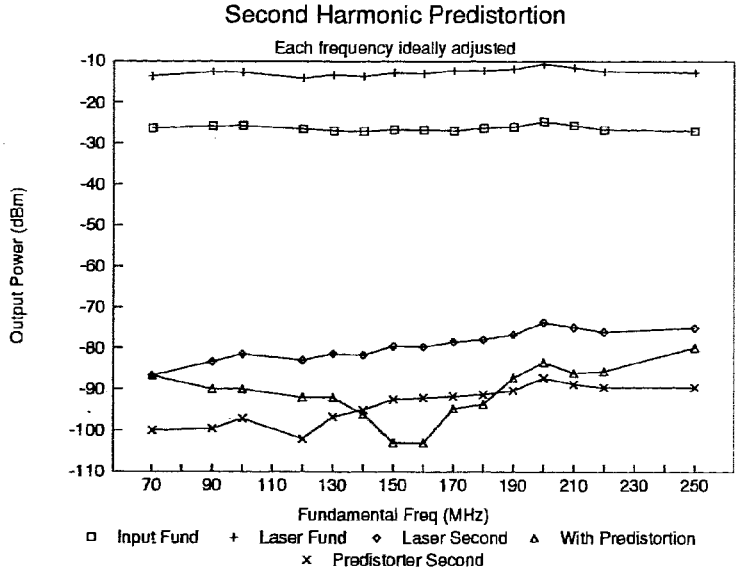

Figure 6.1.1: Measured Second Harmonic Predistortion with adjustment at each frequency

The predistorter could reduce the second harmonic of the laser from 0 dB to 23 dB over a bandwidth from 70 MHz to 250 MHz. The amplitude of the predistorter second harmonic followed the shape of the amplitude of the second harmonic from the laser across the frequency band as expected. Also, maximum cancellation occurred at

around 150 MHz, and decreased on both sides of 150 MHz. This result matches the predistorter phase vs laser phase plot in Figure 5.6.1, which showed that the predistorter phase was correct at around 150 MHz, and then slowly diverged, with the worst diversion occurring at the low frequencies. More cancellation at the low frequencies could have been achieved if the power level of the predistorter second harmonic could have been reduced. At these frequencies, the attenuator was at its maximum attenuation value.

Figures 6.1.2 and 6.1.3 show the reduction in the second harmonic when the predistorter attenuator was fixed at the optimal point for input power levels of -10 dBm and -15 dBm, respectively. Note that the bandwidth over which cancellation occurs has been reduced since the amplitude imbalance at the low frequencies is too large to cause cancellation and actually starts to increase the level of the distortion.

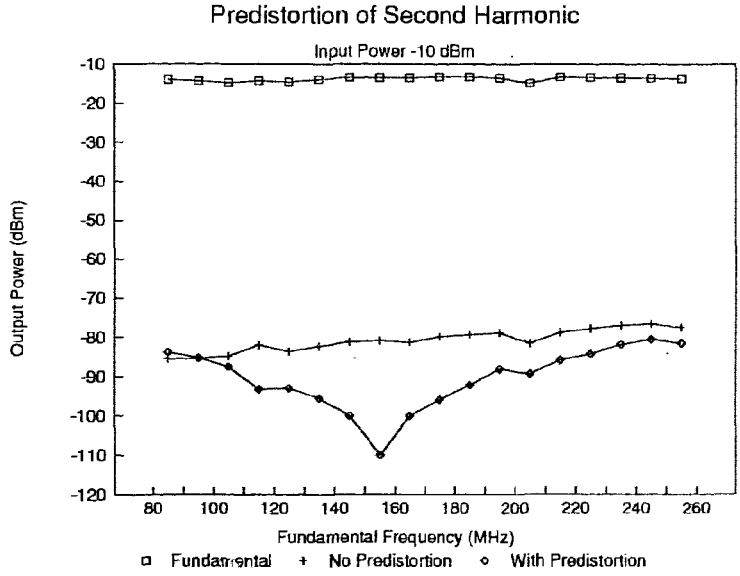

Figure 6.1.2: Measured Second Harmonic Predistortion with Attenuator Fixed. Input -10 dBm.

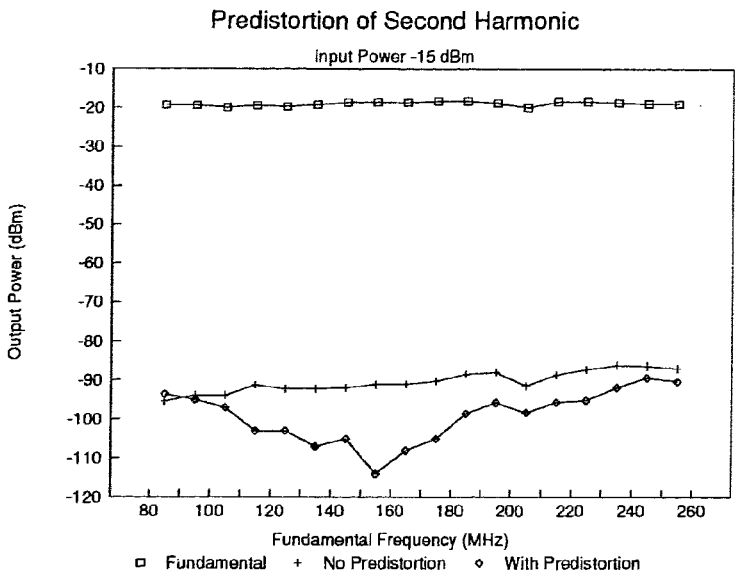

Figure 6.1.3: Measured Second Harmonic Predistortion with Attenuator Fixed. Input -15 dBm.

The amount of cancellation remained approximately the same when the power was reduced. This shows that the laser and predistorter non-linearities are amplitude dependent. Also, it means that the predistorter can predistort the laser at both low and high modulation indices provided that the distortion is not clipping induced.

The results also correspond well to the difference between the optimum predistorter and the actual predistorter as to the range of predistortion and the amount of cancellation. In the next section, a multi-channel test was performed.

6.2 Complete CATV Predistortion of Composite Second Order

The predistorter and laser were then tested using a standard 40 channel CATV test setup which consisted of a matrix generator producing randomly phased tones (CW carriers) at the standard CATV frequencies as the input to the system. The CSO was measured on channel 40 at a variety of modulation indices. At the lower modulation indices, where predistortion was possible, improvement of up to 12 dB was measured. Figure 6.2.1 plots the measured CSO with and without predistortion versus the modulation index. The CSO limit due to clipping is also shown.

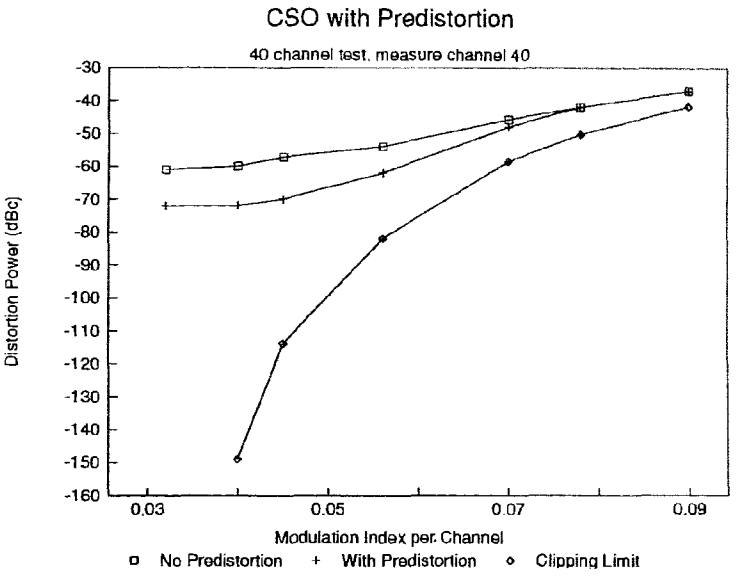

Figure 6.2.1: Measured CSO for 40 Channel Test

The measured CSO with and without predistortion showed the trends expected from the plots in Section 3.4. The predistorter was unable to reduce the CSO at high modulation indices where clipping distortion dominated. Only at modulation indices below 0.07 did the predistorter improve the CSO level.

The measured CSO at high modulation indices was higher than the clipping limit and was attributed to measurement error and the actual operation of the laser diode. The particular laser diode used for testing created considerable noise at higher modulation indices and made the measurements more difficult.

The CSO was also measured at three frequencies across the band. For a modulation index of approximately 0.055, the CSO was measured at 55 MHz, 187 MHz, and 325 MHz with and without the predistorter. Table 6.2.1 summarizes the results.

Table 6.2.1: CSO Measurements

Freq	CSO (dBc)	CSO with PD (dBc)
55 MHz	-66.3	-71.3
187 MHz	-58.9	-68.9
325 MHz	-54.1	-65.1

The CSO was reduced by 5 dB at 55 MHz to 11 dB at 325 MHz. Thus, even though the predistorter worked well only for input frequencies between around 100 MHz to 250 MHz, the number of distortion beats had been reduced across the band and improved the CSO at frequencies where the direct cancellation of the harmonics was not possible.

A final test was performed to determine whether the predistorter affected the CTB of the laser. The CTB was measured at channel 40 at a modulation index of about .045. The CSO without the predistorter was -56 dBc and the CTB was -63.1 dBc. With the predistorter turned on, the CSO dropped to -70 dBc but the CTB increased by 3 dB to -60.1 dBc.

The output of the predistorter was then checked to see if the third order distortion was being caused by the second harmonic generator. When the second harmonic generator variable attenuator was varied, the CSO level could be changed by 13 dB as expected. However, the CTB level stayed constant as the attenuator was varied, which indicated that it was not being generated by the output of the second harmonic generator since the CTB level would have changed by the same ratio as the CSO. The CTB level from the predistorter may have been caused by a reflected third harmonic coming back from the second harmonic generator and passing through the input power splitter and out onto the fundamental path line. Again, isolation between the splitter ports should help to eliminate these effects.

6.3 Adaptive Control of the Predistorter

Over time, the characteristics of the laser and the predistorter will undergo small changes due to temperature drift, aging, and power supply or bias current variations. These variations will affect the overall performance of the system. To account for these variations, the predistorter can be controlled adaptively.

A number of possibilities for adaptive control exist. One method is to characterize the system at different temperatures, and use a temperature sensor to control the attenuator voltage as the temperature varies. Since laser diodes are quite temperature sensitive, this would potentially be quite a good method.

Another method would be to measure the power supply voltage or bias currents to control the predistorter. As with the temperature sensor, the system would have to be characterized at different bias currents to obtain an algorithm to control the attenuator.

A third method is to measure the distortion power at the output of the laser and use it to adaptively control the predistorter attenuator. Since the cancellation has a convergent shape as shown in Figure 6.3.1, the minimum can easily be found. Figure 6.3.1 shows the cancellation of the second harmonic signal for a single tone at 150 MHz vs the attenuator control voltage.

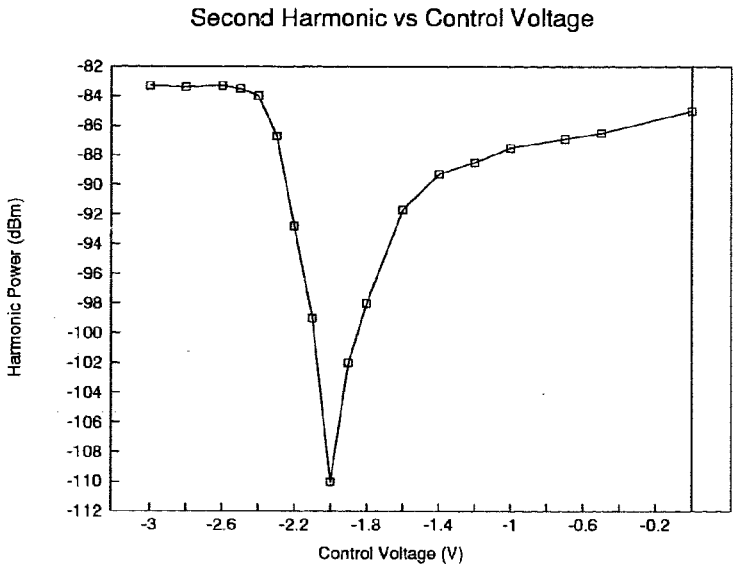

Figure 6.3.1: Second Harmonic Cancellation vs Control Voltage

This curve closely matches the cancellation vs amplitude imbalance graph shown in Figure 4.2.3. An adaptive system would measure the output harmonic power and then adjust the attenuator voltage. If the new voltage results in increased harmonic

power, then the voltage is adjusted in the opposite direction. This process will then eventually settle at the minimum point. Figure 6.3.2 shows an example setup that uses the distortion measurements to adaptively control the predistorter.

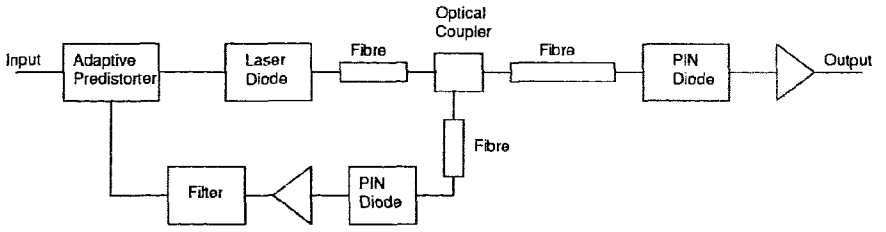

Figure 6.3.2: Block Diagram of Adaptive Predistorter

An optical splitter would be placed after the laser which passed a small percentage of the optical power into a PIN diode. The distortion of the laser seen at the output of the PIN diode would be filtered and amplified to obtain a measure of the NLD in a particular channel. An unused channel would be appropriate for this measurement. Then, the measured distortion power would be used to adapt the predistorter coefficients. This adaptive loop is relatively simple, should be inexpensive to produce, and should provide long-term stability to the predistortion system.

7 CONCLUSION

A third order polynomial model was used to describe a predistorter for an AM-VSB lightwave CATV system. Analytical expressions were derived indicating how much the predistorter would improve the CSO and CTB, and how the predistorter coefficients could be controlled adaptively by making measurements of the total NLD. Also, the analysis showed that the performance of current lasers can be improved using predistortion since the current distortion levels of lasers are still above the signal clipping limit at modulation indices used by the CATV industry.

Then, a predistorter based on the polynomial model was constructed and tested. Preliminary tests performed with a schottky diode as a model for the laser verified the polynomial model results. However, when the laser was characterized, it did not fully obey the analytical model. The distortion amplitude and phase response was frequency dependent and required the predistorter to undergo some modifications in order to predistort the laser.

After the modifications, the predistorter was able to reduce the second order distortion by 3 dB to 20 dB between 50 MHz and 250 MHz, and resulted in the reduction of the CSO in a 40 channel system of up to 12 dB. The third order distortion was not reduced by the predistorter because the predistorter was not able to generate the appropriate signals in its current configuration. However, if the required third order distortion could have been generated, the third order distortion of the laser could also have been reduced.

In terms of further work, new architectures could be investigated for the predistorter so that isolation and back reflection effects do not hinder the operation of the predistorter. This would allow the generation of the small signal levels required for lasers that produce low levels of distortion. Also, construction of the adaptive loop to verify the analytical and measured results should be completed.

Finally, the results of this thesis should be applicable to any type of wideband linearization where the distortion is frequency independent.

8 REFERENCES

[1] Fock, L.S. and Tucker R.S., "Reduction of Distortion in Analogue Modulated Semiconductor Lasers by Feedforward Compensation," *Electron. Lett.*, vol. 27, no. 8, pp. 669-671, 1991

[2] Franckart, J.P. et. al., "Analog Transmission of TV-Channels on Optical Fibers, with Non-linearities Correction by Regulated Feedforward," *Optical Communication: Ninth European Conference on Optical Communication*, pp. 347-350, 1983

[3] Patterson, R.E., Straus, J., Blenman, G., Witkowitz, T., "Linearization of Multichannel Analog Optical Transmitters by Quasi-Feedforward Compensation Technique," *IEEE Trans. Comm.*, vol. 27, no. 3, pp. 582-588, 1979

[4] Childs, R.B., and O'Byrne, V.A., "Predistortion linearization of directly modulated DFB lasers and external modulators for AM video transmission," *Optical Fiber Conference*, pp. 79, 1990

[5] Darcie, T.E. and Bodeep, G.E., "Lightwave Subcarrier CATV Transmission Systems," *IEEE MTT*, vol. 38, no. 5, pp. 524-533, 1990

[6] Bertelsmeier, M. and Zschunke, W., "Linearization of Broadband Optical Transmission Systems by Adaptive Predistortion," *Frequenz*, pp. 206-212, 1984

[7] Darcie, T.E., Lipson, J., Roxlo, C.B., McGrath, C.J., "Fiber Optic Device Technology for Broadband Analog Video Systems," *IEEE LCS Magazine*, pp. 46-52, 1990

[8] Little, F., Pidgeon, R., and Thompson, L, "Performance of AM Multi-Channel Fiber Optic Links," *1989 NCTA Technical Papers*, pp. 1-11, 1989

[9] Rand, H., and Weeks, W., "The AM Fiber Optic Trunk System and Its Key Components," *1989 NCTA Technical Papers*, 1989

[10] Daly, J.C., "Fiber Optic Intermodulation Distortion," *IEEE Trans. Comm.*, vol.30, no. 8, pp. 1954-1958, 1982

[11] Arnold, B., "Third Order Intermodulation Products in a CATV System," *IEEE Trans. Cable Tele.*, vol. 2, no. 2, pp. 67-80, 1977

[12] Shanmugan, K. and Breipohl, A.M., Random Signals: Detection, Estimation and Data Analysis, John Wiley & Sons, Inc., pp. 91, 1988

[13] Wozencraft and Jacobs, Principles of Communication Engineering, McGraw-Hill Book Company, pp. 205-206, 1966

[14] Kandola, G., Analysis and Simulation of an Adaptive Predistorter, M.A.Sc Thesis, School of Engineering Science, SFU, 1991

[15] Saleh, A.A.M., "Fundamental limit on number of channels in SCM lightwave CATV system," *Electron. Lett.*, vol. 25, no. 12, pp 776-777, 1989

[16] Alameh, K. and Minasian, R.A., "Ultimate limits of subcarrier multiplexed lightwave transmission," *Electron. Lett.*, vol. 27, no. 14, pp. 1260-1262, 1991

[17] Frigo, N.J. and Bodeep, G.E., "Clipping Distortion in AM-VSB CATV Subcarrier Multiplexed Lightwave Systems," *IEEE Photon. Technol. Lett.*, vol. 4, no. 7, pp. 781-784, 1992

[18] Shi, Q., Burroughs, R.S., and Lewis, D., "An Alternative Model for Laser Clipping-Induced Nonlinear Distortion for Analog Lightwave CATV Systems," *IEEE Photon. Technol. Lett.*, vol. 4, no. 7, pp. 784-787, 1992

[19] Chung, C.J. and Jacobs, I., "Practical TV Channel Capacity of Lightwave Multichannel AM SCM Systems Limited by the Threshold Nonlinearity of Laser Diodes," *IEEE Photon. Technol. Lett.*, vol 4, no. 3, pp. 289-292, 1992

[20] Photon Systems Corp., 7775 Lougheed Hwy, Burnaby, British Columbia, Canada

[21] MicroSim Corporation, 20 Fairbanks, Irvine, California 92718, 1989

[22] EEsof, Inc., 5795 Lindero Canyon Road, Westlake Village, California 91362, 1989

APPENDIX A - Schematic Diagram of Predistorter